Article

EDA2R–NIK signalling promotes muscle atrophy linked to cancer cachexia

https://doi.org/10.1038/s41586-023-06047-y

Received: 5 July 2022

Accepted: 4 April 2023

Published online: 10 May 2023

Check for updates

Sevval Nur Bilgic[1,4], Aylin Domaniku[1,4], Batu Toledo[1], Samet Agca[1], Bahar Z. C. Weber[1], Dilsad H. Arabaci[1], Zeynep Ozornek[1], Pascale Lause[2], Jean-Paul Thissen[2,3], Audrey Loumaye[2,3] & Serkan Kir[1]✉

Skeletal muscle atrophy is a hallmark of the cachexia syndrome that is associated with poor survival and reduced quality of life in patients with cancer[1]. Muscle atrophy involves excessive protein catabolism and loss of muscle mass and strength[2]. An effective therapy against muscle wasting is currently lacking because mechanisms driving the atrophy process remain incompletely understood. Our gene expression analysis in muscle tissues indicated upregulation of ectodysplasin A2 receptor (EDA2R) in tumour-bearing mice and patients with cachectic cancer. Here we show that activation of EDA2R signalling promotes skeletal muscle atrophy. Stimulation of primary myotubes with the EDA2R ligand EDA-A2 triggered pronounced cellular atrophy by induction of the expression of muscle atrophy-related genes *Atrogin1* and *MuRF1*. EDA-A2-driven myotube atrophy involved activation of the non-canonical NFκB pathway and was dependent on NFκB-inducing kinase (NIK) activity. Whereas EDA-A2 overexpression promoted muscle wasting in mice, deletion of either EDA2R or muscle NIK protected tumour-bearing mice from loss of muscle mass and function. Tumour-induced oncostatin M (OSM) upregulated muscle EDA2R expression, and muscle-specific oncostatin M receptor (OSMR)-knockout mice were resistant to tumour-induced muscle wasting. Our results demonstrate that EDA2R–NIK signalling mediates cancer-associated muscle atrophy in an OSM–OSMR-dependent manner. Thus, therapeutic targeting of these pathways may be beneficial in prevention of muscle loss.

Skeletal muscle atrophy is characterized by excessive protein catabolism leading to loss of muscle mass and strength[2]. Muscle loss is associated with ageing (that is, sarcopenia), muscular dystrophies and the cachexia syndrome that is linked to chronic diseases such as cancer and kidney failure. Cachexia involves progressive muscle wasting that is often accompanied by loss of adipose tissue[3]. Cachexia is highly prevalent in patients with lung, gastric, pancreatic and colorectal cancers, in which it leads to marked weight loss and poor quality of life. Patients with cachectic cancer exhibit frailty, reduced response to treatment and poor survival[1]. Without an effective therapy to reverse muscle wasting, cachexia remains a major problem for these patients[4]. A better understanding of tumour-driven mechanisms that promote muscle atrophy is urgently needed to design new therapeutics.

Ectodysplasin A (EDA) is a tumour necrosis factor (TNF) family member involved in ectodermal development. Mutations in the *EDA* gene have been associated with X-linked hypohidrotic ectodermal dysplasia, a congenital disease characterized by abnormalities in the development of skin, hair, nails, teeth and sweat glands[5]. Alternative splicing generates numerous *EDA* transcripts, including the well-known isoforms EDA-A1 and EDA-A2, which differ only by two amino acids missing in EDA-A2. Whereas EDA-A1 binds to the EDAR receptor, EDA-A2 exclusively interacts with the ectodysplasin A2 receptor (EDA2R)[6]. These ligands are produced as transmembrane proteins, but they are also enzymatically cleaved and secreted. Although defects in *EDA* and *EDAR* genes are linked to ectodermal dysplasia[7], deletion of EDA2R does not affect the development of ectodermal tissues and the physiological roles of the EDA-A2–EDA2R pathway remain largely elusive[8].

EDA2R is induced during muscle wasting

We investigated skeletal muscle wasting driven by cachexia-inducing Lewis lung carcinoma (LLC) and B16 melanoma in syngeneic C57BL/6 mice[9,10]. Our gene expression analysis showed significant upregulation of *Eda2r* messenger RNA (mRNA) in skeletal muscles of tumour-bearing mice (Fig. 1a). In fact, by comparing gene expression in different tissues of mice we identified high levels of *Eda-a1* and *Eda-a2* mRNA in skeletal muscle (Extended Data Fig. 1a,b). Whereas *Edar* expression was highest in the skin, *Eda2r* mRNA levels were markedly enriched in skeletal muscle (Extended Data Fig. 1c,d), suggesting a potential role for EDA2R signalling in muscle pathophysiology. Through testing of gene expression in muscle biopsies, we detected elevated *EDA2R* mRNA in a subset of patients with cachectic lung and colorectal cancer

[1]Department of Molecular Biology and Genetics, Koc University, Istanbul, Turkey. [2]Pole of Endocrinology, Diabetology and Nutrition, Institute of Experimental and Clinical Research, Université Catholique de Louvain, Brussels, Belgium. [3]Department of Endocrinology and Nutrition, Cliniques Universitaires Saint-Luc, Brussels, Belgium. [4]These authors contributed equally: Sevval Nur Bilgic, Aylin Domaniku. ✉e-mail: skir@ku.edu.tr

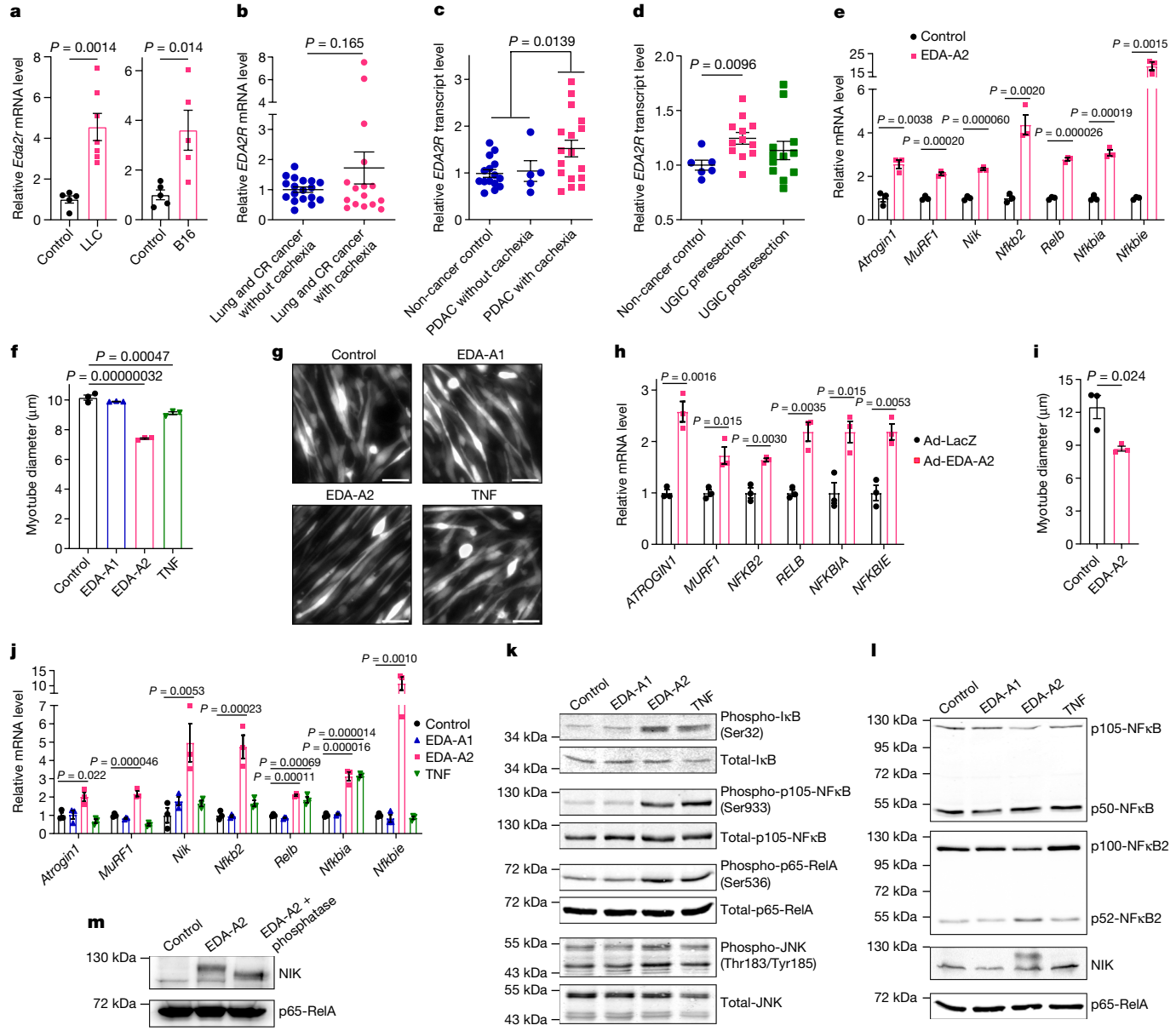

Fig. 1 | EDA-A2 promotes atrophy and activates NFκB signalling in myotubes. **a**,**b**, *Eda2r* mRNA was tested by quantitative PCR with reverse transcription (RT-qPCR) in the gastrocnemius muscle of mice bearing either LLC (16 days) (control, $n = 5$; LLC, $n = 7$) or B16 tumours (14 days) ($n = 5$) (**a**) and in quadriceps muscle biopsies from patients with lung and colorectal (CR) cancer with or without cachexia (with cachexia, $n = 18$; without cachexia, $n = 16$) (**b**). **c**,**d**, The *EDA2R* transcript was analysed in rectus abdominis muscle biopsies from non-cancer controls ($n = 15$), and from patients with PDAC and cachexia ($n = 17$) and with PDAC without cachexia ($n = 5$) (GSE130563) (**c**), and in quadriceps muscle biopsies collected from non-cancer individuals ($n = 6$) and cachectic patients with upper gastrointestinal cancer (UGIC, $n = 12$) before and after tumour resection (GSE34111) (**d**). **e**, Mouse primary myotubes were treated with recombinant EDA-A2 (250 ng ml^{-1} for 24 h) and gene expression was determined by RT-qPCR ($n = 3$). **f**,**g**, Mouse primary myotubes transduced with a green fluorescent protein (GFP) adenovirus were treated with recombinant EDA-A1, EDA-A2 or TNF proteins (250 ng ml^{-1} each, 48 h) and visualized by fluorescence microscopy (**g**). Scale bars, 50 μm. Average myotube diameter was measured ($n = 3$) (**f**). **h**,**i**, Human skeletal muscle myoblasts differentiated into myotubes were treated with either an adenovirus expressing EDA-A2 (**h**) or recombinant EDA-A2 protein (250 ng ml^{-1}, 48 h) (**i**). Gene expression was determined by RT-qPCR ($n = 3$) (**h**) and myotube diameter was measured ($n = 3$) (**i**). **j**–**m**, Mouse primary myotubes were treated with EDA-A1, EDA-A2 or TNF (250 ng ml^{-1} each) for either 24 h (**j**,**l**,**m**) or 10 min (**k**). Gene expression was determined by RT-qPCR ($n = 3$) (**j**). Cell lysates were investigated by immunoblotting (**k**,**l**) and treated with alkaline phosphatase (**m**). Values are mean ± s.e.m. Each dot represents one biological replicate. Data are representative of either two (**h**–**j**) or three (**a**,**e**–**g**,**k**–**m**) independent experiments. Statistical analysis was conducted by either two-tailed unpaired *t*-test (**a**–**c**,**e**,**h**,**i**) or one-way analysis of variance (ANOVA) with Tukey's multiple-comparison test (**d**,**f**,**j**).

(Fig. 1b). Furthermore, our analysis of gene expression datasets indicated significantly increased *EDA2R* transcript levels in muscle biopsies of patients with cachectic pancreatic ductal adenocarcinoma (PDAC) compared with patients with non-cachectic PDAC and non-cancer individuals (Fig. 1c). Similarly, muscle *EDA2R* levels were elevated in cachectic patients with upper gastrointestinal cancers compared with healthy controls. Following tumour resection there was a trend of reduced *EDA2R* expression in these patients (Fig. 1d and Extended Data Fig. 2a). In addition, we also detected a significantly elevated *EDA2R* transcript in muscle biopsies from patients with Duchenne muscular dystrophy (DMD) and facioscapulohumeral muscular dystrophy (FSHD) suffering from reduced muscle mass and function (Extended Data Fig. 2b–d).

Intrigued by these observations, we asked whether the EDA-A2–EDA2R pathway is involved in muscle loss.

EDA2R activation promotes muscle atrophy

First we studied the outcome of the activation of the EDA-A2–EDA2R pathway in muscle cells. For this purpose we isolated primary myoblasts from C57BL/6 mice and differentiated them into fully mature myotube cells. Treatment of primary myotubes with recombinant EDA-A2 protein stimulated mRNA levels of muscle atrophy-related genes *Atrogin1* (*Fbxo32*) and *MuRF1* (*Trim63*) (Fig. 1e). These genes encode E3 ubiquitin ligase enzymes that are well-recognized inducers of muscle protein breakdown[2]. EDA-A2 treatment promoted cellular atrophy in primary myotubes, as evidenced by a reduction in the diameter of these cells (Fig. 1f,g). Whereas primary myotubes did not respond to EDA-A1 treatment, a marginal effect on cellular atrophy was induced by TNF (Fig. 1f,g). Overexpression of EDA-A2, but not EDA-A1, in primary myotubes promoted mRNA levels of *Atrogin1* and *MuRF1* and induced cellular atrophy (Extended Data Fig. 3a–c). In addition, either overexpression of EDA-A2 or the administration of recombinant EDA-A2 also induced *ATROGIN1* and *MURF1* expression in human myotubes and led to a reduction in myotube diameter (Fig. 1h,i and Extended Data Fig. 3d–f). We further documented the atrophic effects of EDA-A2 in mouse primary myotubes by measurement of myosin heavy-chain (MyHC) protein levels. Immunofluorescently labelled MyHC signal dropped significantly following EDA-A2 administration (Extended Data Fig. 3g,h). MyHC downregulation was also detected by immunoblotting. Notably, proteasomal inhibition by MG132 reversed this effect, suggesting the promotion by EDA-A2 of MyHC loss via enhanced proteasomal degradation (Extended Data Fig. 3i).

NFκB pathway downstream of EDA2R

Because previous studies indicated the activation of NFκB signalling by EDA-A2–EDA2R[11,12], we further tested changes in mRNA and protein levels of NFκB factors and their IκB inhibitors. NFκB transcription factors are normally sequestered in the cytoplasm by inhibitory IκB proteins. Canonical NFκB signalling involves IKKβ-dependent phosphorylation of IκBs and their degradation whereas non-canonical (alternative) NFκB activation depends on NFκB-inducing kinase (NIK), which promotes the processing of p100-NFκB2 into the active p52-NFκB2 form resulting in nuclear translocation of the p52-NFκB2–RelB complex[13]. Notably, EDA-A2 administration or overexpression increased mRNA levels of *Nik* (*Map3k14*), *Nfkb2*, *Relb*, *Nfkbia* and *Nfkbie* in mouse primary myotubes (Fig. 1e and Extended Data Figs. 3a and 4a,b). A similar effect was also detected in human myotubes (Fig. 1h and Extended Data Fig. 3e). Compared with TNF, EDA-A2 treatment in mouse primary myotubes promoted a more pronounced effect on the expression of atrophy genes and NFκB signalling elements whereas EDA-A1 failed to stimulate these changes (Fig. 1j). Our results demonstrate that EDA-A2 induces myotube atrophy and the transcription of non-canonical NFκB signalling components, along with high levels of IκBs.

Next we examined activation of the canonical NFκB pathway by determining the phosphorylation of IκB, p105-NFκB and p65-RelA. Treatment of mouse primary myotubes with either EDA-A2 or TNF induced acute phosphorylation of these proteins (Fig. 1k). We also detected an EDA-A2-induced increase in the phosphorylation of JNK, which was previously implicated in EDA2R signalling[11,14] (Fig. 1k). A stable change in the processing of p105-NFκB into p50-NFκB was not detected after 24 h of treatment (Fig. 1l). Interestingly, prolonged treatment of primary myotubes with recombinant EDA-A2 promoted alternative activation of NFκB signalling as evidenced by increased processing of p100-NFκB2 into p52-NFκB2, a process driven by NIK[13]. In fact, EDA-A2 treatment elevated NIK protein levels and specifically induced an electrophoretic mobility shift of this protein (Fig. 1l,m). This shift is in part due to the phosphorylation of NIK because it could be partially suppressed by alkaline phosphatase treatment (Fig. 1m). Other types of post-translational modifications probably contribute to this behaviour. Wild-type (WT) mouse NIK protein overexpressed in primary myotubes also exhibited mobility shift, unlike kinase-dead and autophosphorylation-deficient NIK mutants (Extended Data Fig. 4c). Notably, EDA-A2 treatment increased protein levels of the mutants without inducing a shift. Therefore, EDA-A2-induced mobility shift probably requires intact NIK activity and depends on autophosphorylation of the protein (Extended Data Fig. 4c). This shift was not detected for human NIK protein overexpressed in mouse primary myotubes (Extended Data Fig. 4d). In addition, overexpression of EDA-A2 in primary myotubes also activated alternative NFκB signalling via NIK accumulation (Extended Data Fig. 4e). Our results indicate that EDA-A2 is a potent inducer of atrophy in myotubes, in which it leads to transient and stable activation of the canonical and non-canonical NFκB pathway, respectively.

To distinguish the relative contribution of NFκB pathways to EDA-A2-driven atrophy, we treated primary myotubes with the selective IKKβ inhibitor TPCA-1 and the proteasome inhibitor MG132. We found that EDA-A2-induced phosphorylation of IκB, p105-NFκB and p65-RelA was blocked by TPCA-1 treatment. However, inhibition of the canonical NFκB pathway did not suppress the effects of EDA-A2 on gene expression (Fig. 2a,b). We tested additional IκB phosphorylation inhibitors, including BAY 11-7082 and BOT-64, which also failed to block EDA-A2-induced transcriptional changes (Extended Data Fig. 5a). IκB phosphorylation inhibitors also did not alter p100-NFκB2 processing driven by EDA-A2 (Fig. 2c and Extended Data Fig. 5b). On the other hand, proteasomal inhibition by MG132 was able to prevent p100-NFκB2 processing and the transcriptional effects elicited by EDA-A2 treatment in primary myotubes (Fig. 2a,c), consistent with the implication of alternative NFκB activation downstream of EDA-A2 signalling.

Because EDA-A2 induced mRNA and protein levels of NIK, we compared it with cytokines known to activate NIK, such as BAFF and TWEAK[15]. Whereas BAFF failed to trigger any effect in primary myotubes, EDA-A2 and TWEAK acted similarly because both factors stimulated mRNA expression of the target genes, accumulation of NIK protein and the processing of p100-NFκB2 (Fig. 2d,e). In fact, TWEAK was previously implicated in muscle atrophy[16,17]. Our findings suggest that both factors may use a similar downstream signalling mechanism in myotubes.

NIK activation triggers muscle atrophy

If non-canonical NFκB signalling is involved in muscle atrophy, activation of this pathway alone should stimulate the process. For this purpose we transduced primary myotubes with an adenovirus expressing NIK. Overexpression of NIK promoted the processing of NFκB2 and expression of *Atrogin1*, *MuRF1* and other EDA-A2 targets (Extended Data Fig. 6a and Fig. 2f). In fact, NIK overexpression was sufficient to induce cellular atrophy in primary myotubes (Fig. 2g and Extended Data Fig. 6b). Similar effects on gene expression and cellular atrophy were also observed in human myotubes (Extended Data Fig. 6c–e). We then overexpressed mutant mouse NIK isoforms in mouse primary myotubes. Whereas the kinase-dead mutant did not elicit an effect, the autophosphorylation-deficient mutant triggered partial responses in NFκB2 processing and target gene expression (Extended Data Fig. 6f,g).

We next addressed the necessity of alternative NFκB activation for EDA-A2-driven myotube atrophy. Treatment of primary myotubes with B022, a specific NIK inhibitor[18,19], blocked NIK-induced NFκB2 processing and gene expression in a dose-dependent manner (Extended Data Fig. 7a,b). Combined treatment with B022 and recombinant EDA-A2 also inhibited the expression of *Atrogin1*, *MuRF1* and other EDA-A2 target genes and blunted NFκB2 processing in primary myotubes (Fig. 3a,b). In fact, B022 treatment also blocked the EDA-A2-induced

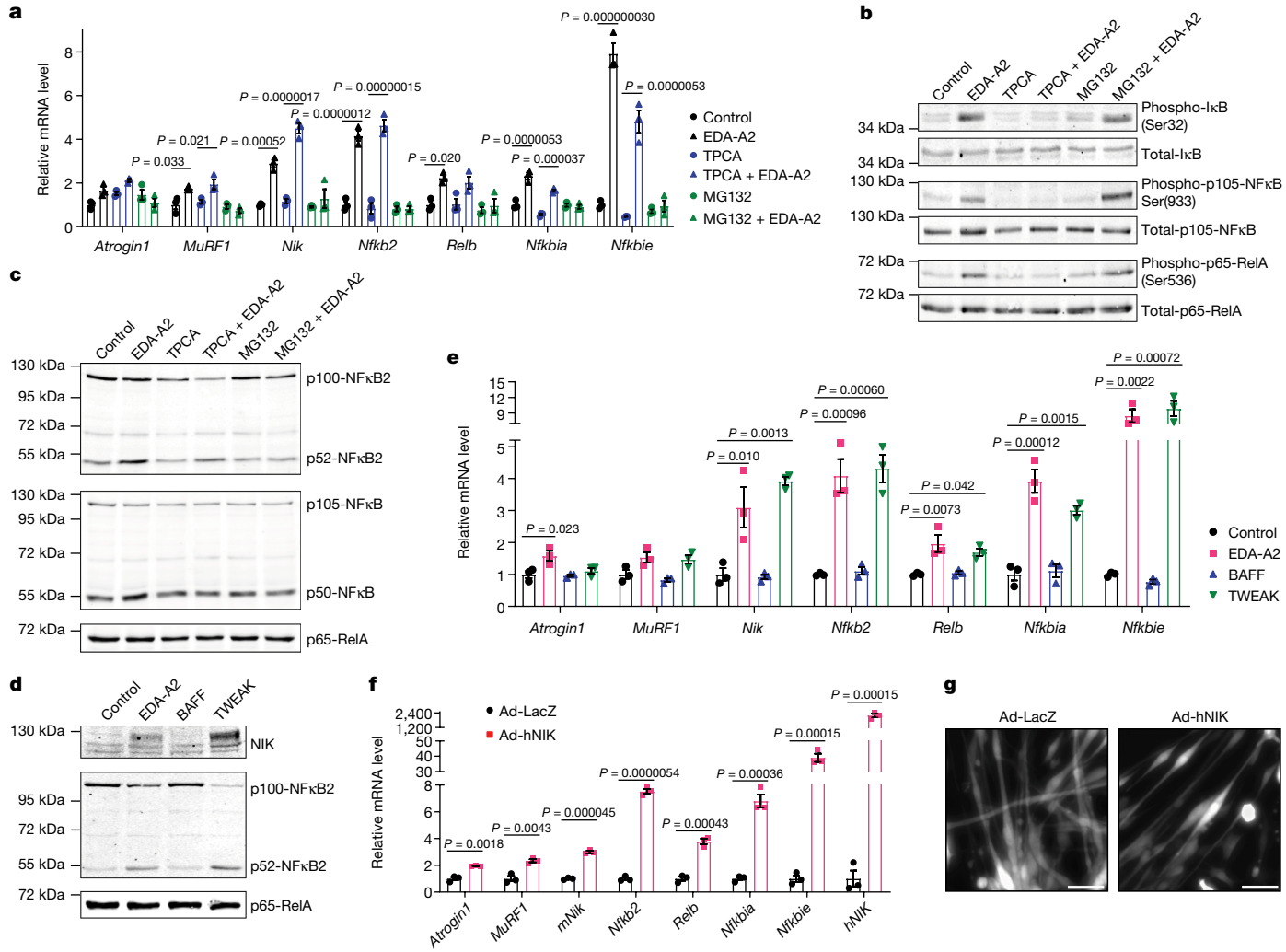

Fig. 2 | Activation of non-canonical NFκB signalling by EDA-A2 or NIK induces atrophy in primary myotubes. a, Mouse primary myotubes were treated with the IKKβ inhibitor TPCA-1 (10 μM), proteasome inhibitor MG132 (5 μM) and EDA-A2 (250 ng ml^{-1}) for 24 h. Changes in gene expression were determined by RT-qPCR ($n = 3$). **b**,**c**, Primary myotubes were treated with either TPCA-1 (10 μM) or proteasome inhibitor MG132 (5 μM) and EDA-A2 (250 ng ml^{-1}) for 10 min (**b**) or 24 h (**c**) and protein levels of NFκB signalling components studied by immunoblotting. **d**,**e**, Primary myotubes were treated with recombinant EDA-A2, BAFF or TWEAK proteins (250 ng ml^{-1} each) for 24 h. Protein levels were determined by immunoblotting (**d**) and gene expression was studied by RT-qPCR ($n = 3$) (**e**). **f**,**g**, Primary myotubes were transduced with adenoviruses expressing LacZ or human NIK (hNIK); 24 h later, changes in gene expression were determined by RT-qPCR ($n = 3$) (**f**). Myotubes also treated with GFP adenovirus were visualized 48 h later under fluorescence microscopy (**g**). Scale bars, 50 μm. Values are mean ± s.e.m. Each dot represents one biological replicate. Data are representative of either two (**d**,**e**) or three (**a**–**c**,**f**,**g**) independent experiments. Statistical analysis was conducted using either one-way ANOVA with Tukey's multiple-comparison test (**a**,**e**) or the two-tailed unpaired *t*-test (**f**).

mobility shift of NIK protein whereas the original NIK signal was massively enhanced, possibly due to a negative feedback loop severed by the inhibition. A similar effect on NIK protein levels was also observed when EDA-A2-overexpressing primary myotubes were treated with B022 (Extended Data Fig. 7c). Furthermore, overexpression of a dominant-negative NIK form that suppressed the NIK-induced processing of NFκB2 also interfered with upregulation of atrophy genes by EDA-A2 (Extended Data Fig. 7d–f). Following NIK inhibition, EDA-A2 was unable to stimulate atrophy in primary myotubes, indicating a major role for NIK signalling in EDA-A2-driven atrophy (Fig. 3c,d).

EDA-A2 overexpression leads to muscle loss

EDA-A2's potent effects on primary myotubes urged us to study its induction in muscle tissue. Previously, transgenic mice overexpressing EDA-A2 in skeletal muscle were generated. These mice exhibited profound muscle degeneration that was prevented by the deletion of EDA2R[8]. Here, we acutely overexpressed EDA-A2 by adenoviral delivery in the tibialis anterior (TA) muscle of mice. Within 7 days the expression of EDA-A2 target genes, including *MuRF1*, *Nik*, *Nfkb2* and *Relb*, was induced in TA muscles (Fig. 3e). Concomitantly, the weight of TA muscles transduced with EDA-A2 adenovirus significantly dropped whereas that of untreated gastrocnemius muscles remained similar (Fig. 3f). Haematoxylin and eosin (H&E) staining of TA muscles showed that muscle fibre cross-sectional area was reduced and the frequency of fibres of small cross-sectional area was increased in response to EDA-A2 overexpression (Fig. 3g–i). These results suggest that EDA-A2 induction is capable of promoting muscle atrophy in vivo.

Tumour-induced muscle loss requires EDA2R

Next we addressed the role of EDA2R–NIK signalling in tumour-induced muscle wasting. We used EDA2R-null (EDA2R-KO) mice, which have

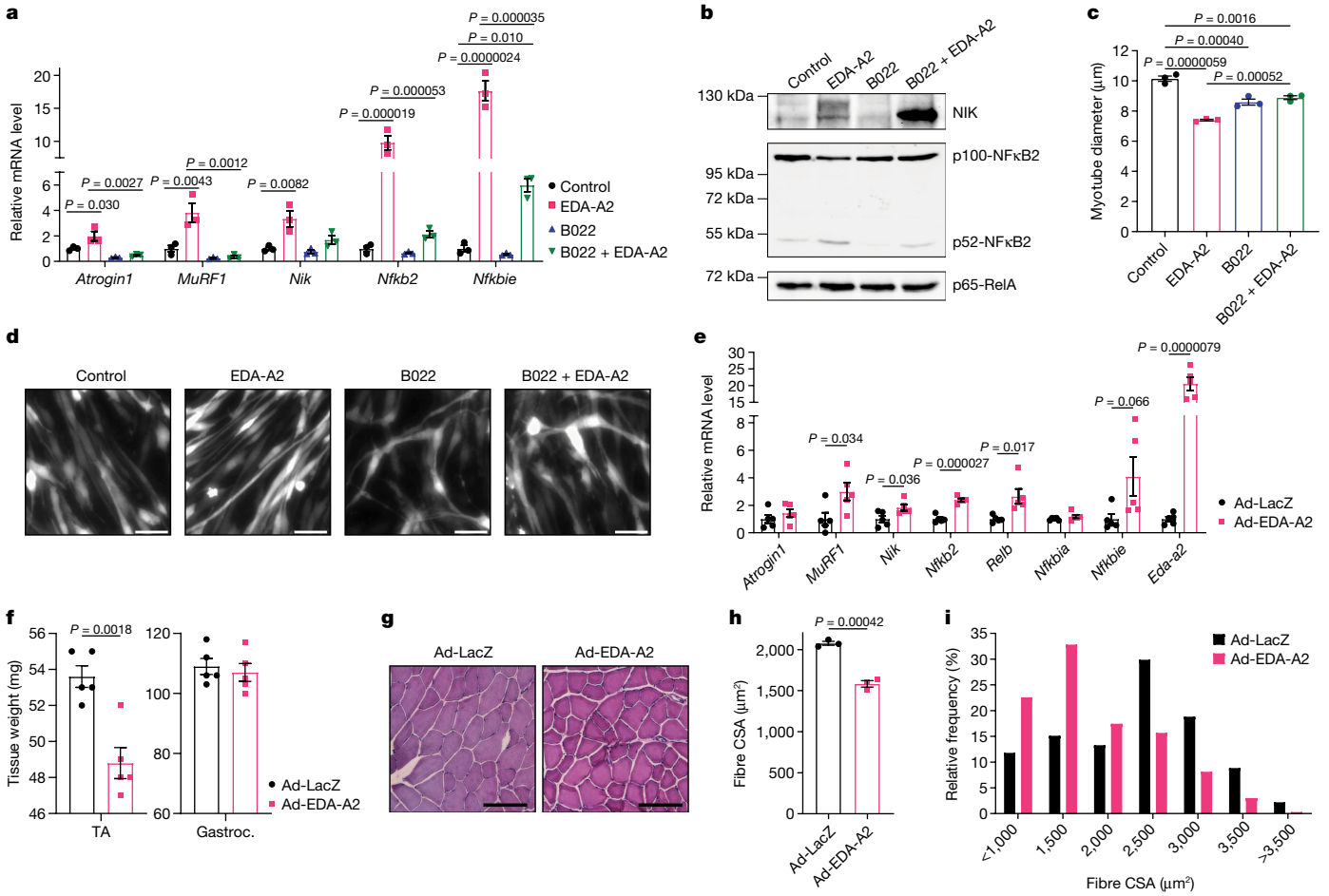

Fig. 3 | EDA-A2-driven muscle atrophy requires NIK activity. a,**b**, Mouse primary myotubes were treated with the NIK inhibitor B022 (5 μM) and EDA-A2 (250 ng ml^{-1}) for 24 h. Changes in gene expression were tested by RT-qPCR ($n = 3$) (**a**) and protein levels determined by immunoblotting (**b**). **c**,**d**, Primary myotubes transduced with GFP adenovirus were treated with B022 (5 μM) and EDA-A2 (250 ng ml^{-1}) for 48 h (**d**). Scale bars, 50 μm. Cells were visualized by fluorescence microscopy and myotube diameter measured ($n = 3$) (**c**). **e**–**i**, The TA muscles of mice were transduced with either LacZ or EDA-A2 adenoviruses. Mice were killed 7 days later ($n = 5$ mice per group). Changes in gene expression of TA muscles were determined by RT-qPCR ($n = 5$ mice) (**e**). TA and gastrocnemius (gastroc.) muscles were weighed ($n = 5$ mice) (**f**). TA muscles were H&E stained (**g**) and their fibre cross-sectional area (CSA) (**h**) and fibre frequency distribution (**i**) were determined ($n = 3$ mice). Scale bars, 100 μm. Values are mean ± s.e.m. Each dot represents one biological replicate. Data are representative of either two (**b**,**g**–**i**) or three (**a**,**c**–**f**) independent experiments. Statistical analysis was conducted using either one-way ANOVA with Tukey's multiple-comparison test (**a**,**c**) or the two-tailed unpaired *t*-test (**e**,**f**,**h**).

normal body weight and lack any obvious phenotypic characteristics[8]. We inoculated littermate WT and knockout (KO) mice with LLC tumours. Remarkably, muscle wasting was attenuated in EDA2R-KO mice as evidenced by the preservation of gastrocnemius and TA muscles (Fig. 4a). Accordingly, these mice had higher tumour-free body weight compared with tumour-bearing WT mice (Extended Data Fig. 8a,b) and they also exhibited improved muscle performance as measured by forelimb grip strength (Fig. 4b). Tumour weight, the expression of immune response-related genes in tumours and plasma C-reactive protein levels (as an indicator of systemic inflammation) were comparable between WT and KO groups (Extended Data Fig. 8b–d). We also dissected and weighed adipose tissue depots, including epididymal and inguinal white adipose tissue and interscapular brown adipose tissue (BAT). However, no specific effect on adipose tissue wasting was detected (Fig. 4a). Similar results for tumour-free body weight, muscle mass and physical strength were obtained when EDA2R-KO mice were inoculated with B16 tumours (Fig. 4c,d and Extended Data Fig. 8e,f).

The improvements noted in muscle mass and function were also reflected in muscle histology. H&E staining of muscle tissue demonstrated an increase in muscle fibre cross-sectional area in tumour-bearing KO mice compared with their WT counterparts (Fig. 4e,f and Extended Data Fig. 8g,h). Tumour-driven enrichment of muscle fibres with small cross-sectional area was suppressed in EDA2R-deficient mice (Fig. 4g and Extended Data Fig. 8i). We also examined changes in the expression of EDA-A2 target genes in these samples. In the absence of EDA2R, tumour-induced mRNA expression of *Atrogin1*, *MuRF1* and *Nik* was suppressed whereas limited induction in *Nfkb2* and *Relb* mRNA levels was detected (Fig. 4h and Extended Data Fig. 8j–l). Furthermore, Atrogin1 and MuRF1 protein levels were also reduced in the muscles of tumour-bearing EDA2R-KO mice (Fig. 4i). These findings indicate that EDA2R function is essential for tumour-induced muscle wasting.

NIK is involved in muscle wasting

To further delineate this pathway, we generated skeletal muscle-specific NIK-KO mice (Myo-NIK-KO). We confirmed that the deletion was restricted to skeletal muscle by comparison of *Nik* mRNA levels in various tissues (Extended Data Fig. 9a). We then inoculated these mice with LLC tumours and studied cachexia phenotypes. Similar to EDA2R-KO

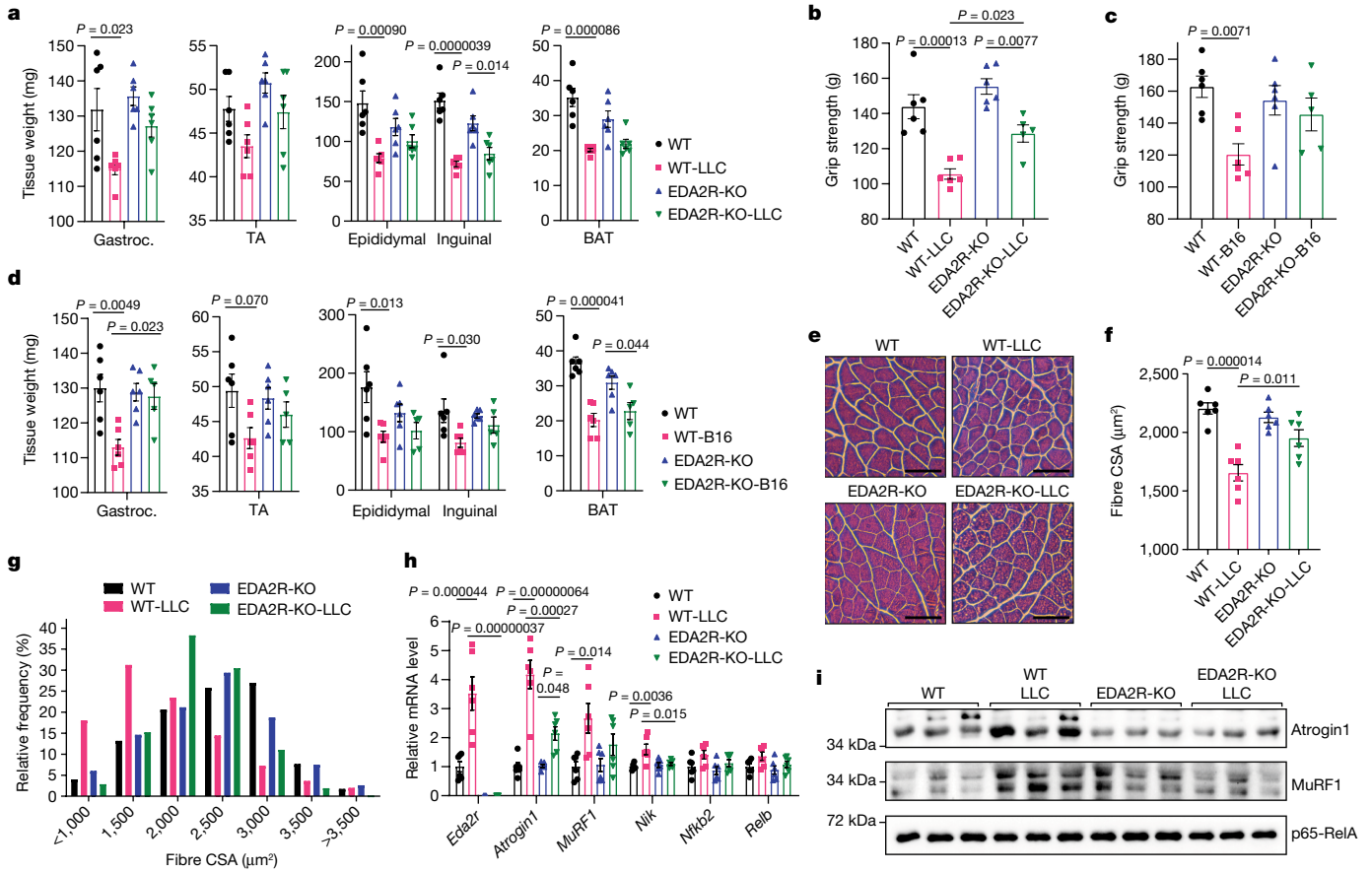

Fig. 4 | EDA2R-deficient mice are resistant to tumour-induced muscle wasting. a,**b**,**e**–**i**, Mice were inoculated with LLC cells and killed 16 days later. Collected tissues were weighed ($n = 6$ mice per group) (**a**). Forelimb grip strength was measured before euthanasia (EDA2R-KO-LLC, $n = 5$; other groups, $n = 6$ mice) (**b**). **c**,**d**, Mice were inoculated with B16 cells and killed 14 days later (EDA2R-KO-B16, $n = 5$ mice; other groups, $n = 6$). Forelimb grip strength was measured before euthanasia (**c**). Collected tissues were weighed (**d**). **e**–**g**, Gastrocnemius muscle cross-sections were H&E stained (**e**) and cross-sectional area (**f**) and fibre frequency distribution (**g**) measured ($n = 6$ mice). Scale bars, 100 μm. **h**,**i**, Gastrocnemius muscle mRNA levels were tested by RT-qPCR ($n = 6$ mice) (**h**) and their protein levels determined by immunoblotting ($n = 3$ mice) (**i**). Values are mean ± s.e.m. Each dot represents one biological replicate. **a**–**i**, Data are representative of three independent experiments. **a**–**d**,**f**,**h**, Statistical analysis was conducted using two-way ANOVA with Tukey's multiple-comparison test.

mice, Myo-NIK-KO mice were also resistant to tumour-induced weight loss (Extended Data Fig. 9b,c). The absence of NIK in muscles of tumour-bearing mice prevented the loss of muscle mass and preserved muscle function as determined by muscle weight and forelimb grip strength measurements, respectively (Extended Data Fig. 9d,e). No specific effect on adipose tissue wasting was observed (Extended Data Fig. 9d). Examination of muscle histology in tumour-bearing mice also demonstrated an increase in muscle fibre cross-sectional area and a decrease in the frequency of fibres of small cross-sectional area in Myo-NIK-KO mice compared with their WT counterparts (Extended Data Fig. 9f–h). Analysis of gene expression in muscle tissues also demonstrated a reduction in tumour-induced mRNA and protein levels of Atrogin1 and MuRF1 in the KO mice (Extended Data Fig. 9i–k). The similarities in tumour-driven responses shared by Myo-NIK-KO and EDA2R-KO mice suggest that a common pathway involving EDA2R–NIK acts to promote muscle atrophy.

EDA2R is upregulated by oncostatin M

We also investigated how tumours upregulate *Eda2r* expression in muscle tissue. Through testing of various tumour-induced cytokines on primary myotubes, we observed *Eda2r* upregulation by oncostatin M (OSM; Fig. 5a and Extended Data Fig. 10a), an IL-6 family cytokine involved in a variety of biological processes including muscle atrophy[20,21]. When overexpressed in TA muscles of mice, OSM significantly increased *Eda2r* mRNA (Fig. 5b). Analysis of blood plasma from LLC tumour-bearing mice detected elevated OSM levels (Fig. 5c), implying that tumour-induced OSM may activate EDA2R signalling in muscle tissue. In fact, treatment of mouse primary myotubes with recombinant OSM protein also stimulated the expression of *Atrogin1* and resultant cellular atrophy, indicating that OSM itself is an atrophy-inducing factor (Fig. 5d and Extended Data Fig. 10b,c). We found that combined treatment of OSM and EDA-A2 resulted in atrophy-related gene expression in primary myotubes in an additive manner. After testing changes in mRNA levels of OSM target genes *Osmr* and *Socs3*, EDA-A2-specific targets *MuRF1*, *Nik*, *Nfkb2* and *Relb* and OSM–EDA-A2 common gene targets *Atrogin1* and *Ampd3*, we detected additive effects on the expression of *Atrogin1*, *Ampd3* and *Osmr* (Fig. 5d and Extended Data Fig. 10d). The combination of OSM and EDA-A2 also caused a further reduction in myotube diameter (Extended Data Fig. 10b,c). These secreted factors may operate alone or together to induce atrophy of cultured myotubes.

Tumour-induced muscle loss requires OSMR

To determine the role of OSM in EDA2R regulation and muscle wasting, we generated skeletal muscle-specific OSM receptor (OSMR) KO (Myo-OSMR-KO) mice. We confirmed the depletion of OSMR

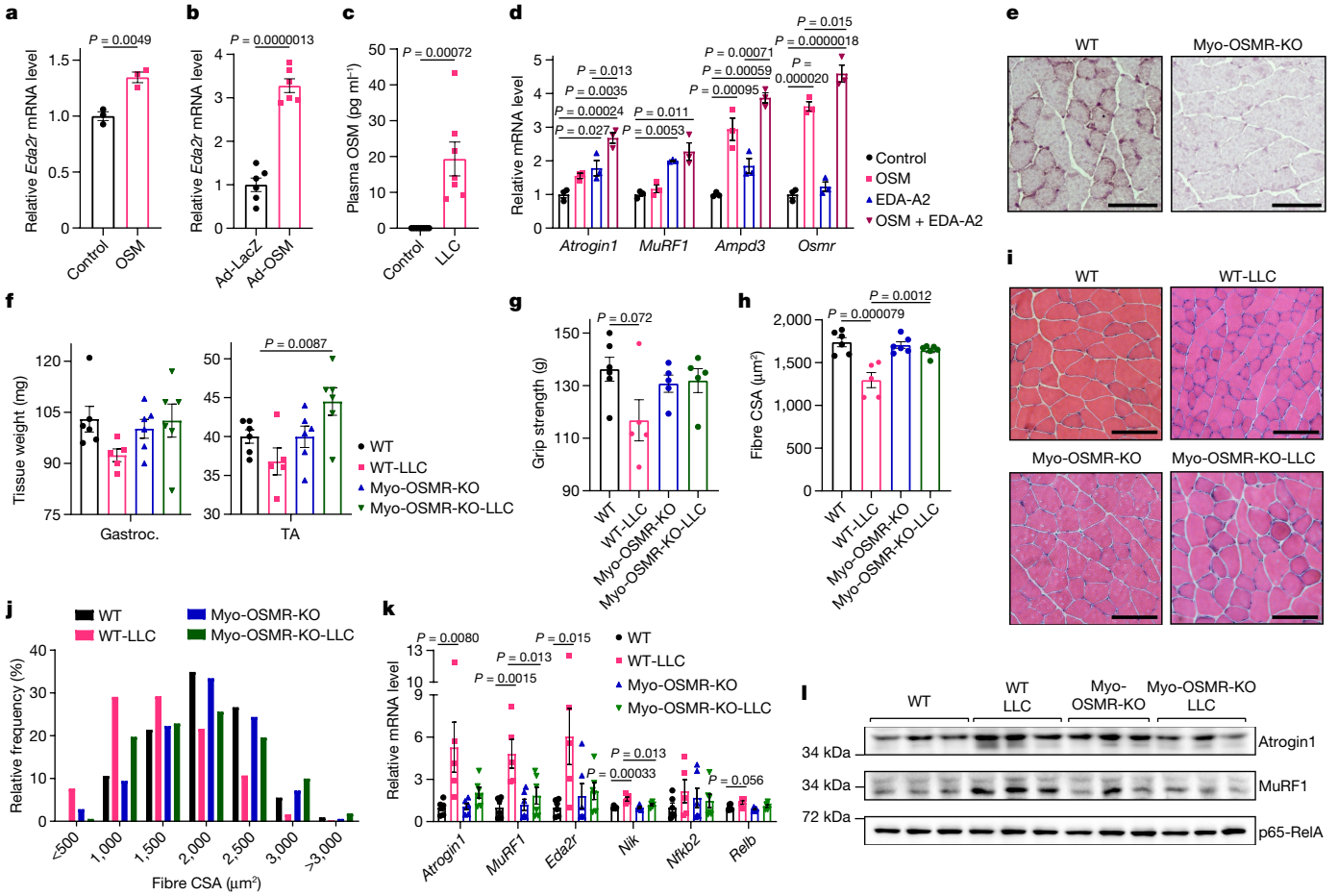

Fig. 5 | OSM induces *Eda2r* expression in muscle and depletion of OSMR protects from muscle wasting. a, Mouse primary myotubes were treated with recombinant OSM (250 ng ml^{-1}) for 6 h ($n = 3$). **b**, Tibialis anterior muscles of mice were transduced with LacZ or OSM adenoviruses and mice were killed 7 days later. mRNA levels were determined by RT-qPCR ($n = 6$ mice). **c**, Mice were inoculated with LLC cells and killed 16 days later. Plasma OSM levels were measured by ELISA (control, $n = 8$ mice; LLC, $n = 7$). **d**, Mouse primary myotubes were treated with recombinant OSM (250 ng ml^{-1} for 48 h) and EDA-A2 (100 ng ml^{-1} for 24 h). Changes in gene expression were determined by RT-qPCR ($n = 3$). **e**, OSMR levels in gastrocnemius muscle were determined by immunohistochemistry. **f**–**l**, Mice were inoculated with LLC cells and killed 16 days later (WT-LLC, $n = 5$ mice; other groups, $n = 6$). Collected tissues were weighed (**f**). Forelimb grip strength was measured before euthanasia (WT, $n = 6$ mice; other groups, $n = 5$) (**g**). Gastrocnemius muscle cross-sections were H&E stained (**i**), and cross-sectional area (**h**) and fibre frequency distribution (**j**) were measured (WT-LLC, $n = 5$ mice; other groups, $n = 6$). Scale bars, 100 μm. **k**,**l**, Gastrocnemius muscle mRNA levels were tested by RT-qPCR (WT-LLC, $n = 5$ mice; other groups, $n = 6$) (**k**) and their protein levels determined by immunoblotting ($n = 3$ mice) (**l**). Values are mean ± s.e.m. Each dot represents one biological replicate. Data are representative of either two (**a**,**c**–**e**) or three (**b**,**f**–**l**) independent experiments. Statistical analysis was conducted using either the two-tailed unpaired *t*-test (**a**–**c**), one-way ANOVA with Tukey's multiple-comparison test (**d**) or two-way ANOVA with Tukey's multiple-comparison test (**f**–**h**,**k**).

in muscle fibres using immunohistochemistry (Fig. 5e). Following LLC tumour inoculation, Myo-OSMR-KO mice were protected from weight loss and muscle wasting (Fig. 5f and Extended Data Fig. 10e,f) but tumour-bearing KO mice lost adipose tissue mass (Extended Data Fig. 10g). Muscle strength, as assessed by forelimb grip measurement, reflected the preservation of muscle mass in KO mice whereas WT mice exhibited evident reduced performance (Fig. 5g). H&E staining of gastrocnemius tissue sections indicated that tumour-bearing Myo-OSMR-KO mice had significantly wider muscle fibres than tumour-bearing controls (Fig. 5h,i); fibres of small cross-sectional area were enriched in the latter group (Fig. 5j). Gene expression analysis demonstrated that tumour-induced mRNA and protein levels of Atrogin1 and MuRF1 were reduced in the muscles of Myo-OSMR-KO mice compared with their WT counterparts (Fig. 5k,l and Extended Data Fig. 10h). Importantly, OSMR depletion also suppressed the upregulation of *Eda2r* and its downstream targets in these samples (Fig. 5k and Extended Data Fig. 10h). These findings suggest that the OSM–OSMR pathway plays a major role in tumour-induced muscle wasting, including the activation of EDA2R–NIK signalling.

Discussion

Taken together, our findings indicate that EDA2R signalling is a potent inducer of muscle atrophy. Whereas the EDA-A1–EDAR pathway is important for the development of ectodermal structures, EDA-A2–EDA2R signalling is involved in skeletal muscle pathophysiology[8]. EDA2R expression is upregulated in muscles of tumour-bearing mice and also in muscle biopsies of patients with cachectic cancer. Previously, chronic activation of EDA2R signalling was shown to cause myodegeneration in EDA-A2 transgenic mice[8]. Our results demonstrate that EDA2R upregulation in cancer cachexia contributes to muscle loss. Canonical NFκB signalling has been shown to promote muscle protein breakdown[2]. The present study indicates that non-canonical NFκB activation also triggers muscle atrophy in which NIK plays a central role. Deletion of either EDA2R or NIK in mice was sufficient to confer resistance against tumour-induced muscle wasting. EDA2R expression is induced by inflammatory cytokines, and we identified OSM as a prominent regulator. In fact, depletion of OSMR in muscle protected against wasting of this tissue. Our results suggest that OSM–OSMR

signalling acts in parallel with the EDA2R–NIK pathway and reinforces muscle atrophy and EDA2R upregulation. Additional studies using muscle biopsies and blood samples from weight-losing cancer patients are needed to establish the clinical impact of the activation of these pathways in cancer cachexia.

Systemic inflammation has been implicated to play a major role in cancer cachexia, with pro-inflammatory cytokines TNF, IL-1 and IL-6 described as causal agents[22]. However, clinical trials testing anti-TNF therapies failed to prevent muscle atrophy in patients with advanced cancer cachexia[23,24]. Although anti-IL-1 and anti-IL-6 therapies showed promising results in patients with cachectic cancer, a satisfactory effect on skeletal muscle mass was not achieved[25,26]. An effective therapy against cachexia-associated muscle wasting is urgently needed. Our findings suggest that EDA2R–NIK and OSM–OSMR pathway elements may serve as new therapeutic targets. Prospective studies should test the pharmacologic inhibition of these pathways in prevention of muscle wasting. Blockade of EDA2R or OSMR and inhibition of NIK may be useful in reversal of muscle loss. Because pathways parallel to EDA-A2–EDA2R, such as TWEAK–FN14, may also use NIK to promote muscle atrophy, NIK inhibition is a preferable choice. However, the ubiquitous expression of NIK in the body and its prominent roles in immunity may limit this strategy. Interestingly, depletion of muscle OSMR was sufficient to both attenuate muscle loss and silence EDA2R activation, making the OSM–OSMR pathway a potentially attractive therapeutic target.

EDA-A2 was previously shown to contribute to obesity-related glucose intolerance, possibly through promotion of insulin resistance in muscle[14]. Because impaired glucose metabolism during cancer cachexia has also been reported[27], it is possible that inhibition of the EDA2R–NIK pathway may improve cachexia-related abnormalities in glucose metabolism. Furthermore, our gene expression analysis demonstrated elevated *EDA2R* mRNA in muscle biopsies from patients with muscular dystrophy, and *EDA2R* upregulation was also reported in the muscles of ageing individuals[28]. It is likely that the role of EDA2R–NIK in muscle atrophy is not restricted to cancer cachexia, and therapeutic targeting of this pathway may thus be beneficial in other muscle disorders.

Online content

Any methods, additional references, Nature Portfolio reporting summaries, source data, extended data, supplementary information, acknowledgements, peer review information; details of author contributions and competing interests; and statements of data and code availability are available at https://doi.org/10.1038/s41586-023-06047-y.

1. Baracos, V. E., Martin, L., Korc, M., Guttridge, D. C. & Fearon, K. C. H. Cancer-associated cachexia. *Nat. Rev. Dis. Primers* **4**, 17105 (2018).
2. Cohen, S., Nathan, J. A. & Goldberg, A. L. Muscle wasting in disease: molecular mechanisms and promising therapies. *Nat. Rev. Drug Discov.* **14**, 58–74 (2015).
3. Argiles, J. M., Stemmler, B., Lopez-Soriano, F. J. & Busquets, S. Inter-tissue communication in cancer cachexia. *Nat. Rev. Endocrinol.* **15**, 9–20 (2018).
4. Dolly, A., Dumas, J. F. & Servais, S. Cancer cachexia and skeletal muscle atrophy in clinical studies: what do we really know? *J. Cachexia Sarcopenia Muscle* **11**, 1413–1428 (2020).
5. Kowalczyk-Quintas, C. & Schneider, P. Ectodysplasin A (EDA) – EDA receptor signalling and its pharmacological modulation. *Cytokine Growth Factor Rev.* **25**, 195–203 (2014).
6. Yan, M. et al. Two-amino acid molecular switch in an epithelial morphogen that regulates binding to two distinct receptors. *Science* **290**, 523–527 (2000).
7. Sadier, A., Viriot, L., Pantalacci, S. & Laudet, V. The ectodysplasin pathway: from diseases to adaptations. *Trends Genet.* **30**, 24–31 (2014).
8. Newton, K., French, D. M., Yan, M., Frantz, G. D. & Dixit, V. M. Myodegeneration in EDA-A2 transgenic mice is prevented by XEDAR deficiency. *Mol. Cell. Biol.* **24**, 1608–1613 (2004).
9. Das, S. K. et al. Adipose triglyceride lipase contributes to cancer-associated cachexia. *Science* **333**, 233–238 (2011).
10. Kir, S. et al. Tumour-derived PTH-related protein triggers adipose tissue browning and cancer cachexia. *Nature* **513**, 100–104 (2014).
11. Sinha, S. K., Zachariah, S., Quinones, H. I., Shindo, M. & Chaudhary, P. M. Role of TRAF3 and -6 in the activation of the NF-kappa B and JNK pathways by X-linked ectodermal dysplasia receptor. *J. Biol. Chem.* **277**, 44953–44961 (2002).
12. Verhelst, K. et al. XEDAR activates the non-canonical NF-kappaB pathway. *Biochem. Biophys. Res. Commun.* **465**, 275–280 (2015).
13. Liu, T., Zhang, L., Joo, D. & Sun, S. C. NF-kappaB signaling in inflammation. *Signal Transduct. Target Ther.* https://doi.org/10.1038/sigtrans.2017.23 (2017).
14. Awazawa, M. et al. A microRNA screen reveals that elevated hepatic ectodysplasin A expression contributes to obesity-induced insulin resistance in skeletal muscle. *Nat. Med.* **23**, 1466–1473 (2017).
15. Valino-Rivas, L. et al. NIK as a druggable mediator of tissue injury. *Trends Mol. Med.* **25**, 341–360 (2019).
16. Dogra, C. et al. TNF-related weak inducer of apoptosis (TWEAK) is a potent skeletal muscle-wasting cytokine. *FASEB J.* **21**, 1857–1869 (2007).
17. Johnston, A. J. et al. Targeting of Fn14 prevents cancer-induced cachexia and prolongs survival. *Cell* **162**, 1365–1378 (2015).
18. Ren, X. et al. A small-molecule inhibitor of NF-kappaB-inducing kinase (NIK) protects liver from toxin-induced inflammation, oxidative stress, and injury. *FASEB J.* **31**, 711–718 (2017).
19. Li, X. et al. Activation of NF-kappaB-inducing kinase in islet beta cells causes beta cell failure and diabetes. *Mol. Ther.* **28**, 2430–2441 (2020).
20. Richards, C. D. The enigmatic cytokine oncostatin m and roles in disease. *ISRN Inflamm.* **2013**, 512103 (2013).
21. Miki, Y. et al. Oncostatin M induces C2C12 myotube atrophy by modulating muscle differentiation and degradation. *Biochem. Biophys. Res. Commun.* **516**, 951–956 (2019).
22. Webster, J. M., Kempen, L., Hardy, R. S. & Langen, R. C. J. Inflammation and skeletal muscle wasting during cachexia. *Front. Physiol.* **11**, 597675 (2020).
23. Jatoi, A. et al. A placebo-controlled double blind trial of etanercept for the cancer anorexia/weight loss syndrome: results from N00C1 from the North Central Cancer Treatment Group. *Cancer* **110**, 1396–1403 (2007).
24. Jatoi, A. et al. A placebo-controlled, double-blind trial of infliximab for cancer-associated weight loss in elderly and/or poor performance non-small cell lung cancer patients (N01C9). *Lung Cancer* **68**, 234–239 (2010).
25. Bayliss, T. J., Smith, J. T., Schuster, M., Dragnev, K. H. & Rigas, J. R. A humanized anti-IL-6 antibody (ALD518) in non-small cell lung cancer. *Expert Opin. Biol. Ther.* **11**, 1663–1668 (2011).
26. Marceca, G. P., Londhe, P. & Calore, F. Management of cancer cachexia: attempting to develop new pharmacological agents for new effective therapeutic options. *Front. Oncol.* **10**, 298 (2020).
27. Honors, M. A. & Kinzig, K. P. The role of insulin resistance in the development of muscle wasting during cancer cachexia. *J. Cachexia Sarcopenia Muscle* **3**, 5–11 (2012).
28. Barbera, M. C. et al. Increased expression of ectodysplasin A2 receptor EDA2R is the most remarkable and ubiquitous aging-related transcriptional hallmark. Preprint at https://doi.org/10.21203/rs.3.rs-774469/v1 (2021).

Methods

Reagents

Recombinant proteins were purchased from R&D Systems: EDA-A1 (no. 3944-ED), EDA-A2 (no. 922-ED), TNF (no. 410-MT), BAFF (no. 8876-BF), TWEAK (no. 1237-TW), OSM (no. 495-MO), IL-6 (no. 406-ML) and LIF (no. 8878-LF). Small-molecule inhibitors were acquired from the following sources: TPCA-1 (abcam, no. ab145522), MG132 (Sigma, no. M8699), BAY 11-7082 (abcam, no. ab141228), BOT-64 (Santa Cruz, no. sc-222062) and B022 (Aobious, no. AOB8699). Mouse EDA-A1 (no. MC208411), mouse EDA-A2 (no. MC208415) and mouse OSM (no. MR226014) expression plasmids were purchased from Origene. Mouse NIK expression plasmid was purchased from Invivogen (no. pUNO1-mMap3k14). WT human NIK and NIK-K429/430A mutant plasmids were a gift from M. Kracht (JLU Giessen).

Mice

Mice were housed at 22 °C and 50% humidity with a 12/12 h light/dark cycle (07:00–19:00) and given ad libitum access to a standard rodent chow diet and water. Male mice 8–12 weeks old were used in all animal experiments. Mice were kept in the Koc University Animal Research Facility in accordance with institutional policies and animal care ethics guidelines. A minimum sample size of four, determined empirically by performing preliminary experiments, was chosen to ensure that adequate statistical power was achieved. Mice were divided randomly into treatment groups, also satisfying the criterion that average body weight in each group be similar. The investigators were blinded to group allocation during data collection, which was shown during data analysis. EDA2R-KO and NIK-floxed mice were generated by Genentech[8,29]; NIK-floxed mice were a gift from S.-C. Sun (MD Anderson Cancer Center) and Myo-NIK-KO mice were generated by crossing NIK-floxed and ACTA1-Cre mice (Jackson strain no. 006149). OSMR-floxed mice (strain no. 011081) were purchased from Jackson laboratory. Myo-OSMR-KO mice were generated by crossing OSMR-floxed and ACTA1-Cre mice (Jackson strain no. 006149). All mice were maintained on a pure C57BL/6 background. Plasma C-reactive protein levels were measured using an ELISA assay (BT Lab, no. E0218Mo). All animal protocols were approved by the Institutional Animal Care and Use Committee of Koc University. For all tumour inoculation experiments and in line with Institutional Animal Care and Use Committee guidelines, humane endpoints were determined as maximal tumour size of 2 cm (the longest tumour length), at least 15% body weight loss and severe lethargy. These limits were not exceeded in any of the experiments.

Tumour inoculation

Lewis lung carcinoma and B16 (B16-F10) cells were cultured in DMEM medium (Sigma, no. 5796) with 10% fetal bovine serum (FBS) and penicillin-streptomycin (Invitrogen). B16 cells were also supplemented with freshly added 2 mM L-glutamine (Invitrogen). Cell lines were acquired from ATCC and were not authenticated. Mice were divided randomly into groups while also satisfying the criterion that the average body weight in each group be similar. All mice used in tumour inoculation experiments, including transgenic lines, were from the C57BL/6 background. LLC cells (5×10^6 per mouse) or B16 cells (2.5×10^6 per mouse) were injected subcutaneously over the flank. Non-tumour-bearing control mice received vehicle (PBS) only. Mice were housed individually in all tumour inoculation experiments. Mice were killed either at 16 days (LLC) or 14 days (B16) after tumour inoculation. Epididymal, inguinal and interscapular fat depots, gastrocnemius and TA muscles and tumours were dissected and weighed using an analytical balance.

Grip strength

Forelimb grip strength was measured on the same day as euthanasia. Each mouse was allowed to grab a bar attached to a force transducer while being steadily pulled horizontally by the tail away from the bar (Ugo Basile grip strength meter). The maximum strength produced before releasing the bar registered from at least three repetitions was averaged to determine the grip strength of each mouse.

Tissue histology

Isopentane was cooled by liquid nitrogen until two-thirds frozen. Muscle samples wrapped in aluminium foil were placed in cooled isopentane for 15–20 s. Frozen tissues were embedded in Tissue-Tek OCT freezing medium (Sakura) in cryomoulds. Using a cryostat, 8-µm-thick sections were cut and collected on Superfrost Plus slides (Thermo). Sections were fixed with 4% paraformaldehyde and treated with haematoxylin (Merck, no. 105174), 0.1% HCl, eosin (Merck, no. 109844), a 70–100% ethanol gradient and xylene (Isolab), respectively. Muscle fibre cross-sectional area was measured using Image J software.

Immunohistochemistry

Cryosections (5 µm) were fixed with neutral buffer formalin and then incubated with 0.3% hydrogen peroxide for 10 min to block endogenous peroxidase activity. Sections were incubated in blocking solution (3% bovine serum albumin + 0.1% Triton X-100 + 5% horse serum) at room temperature for 1 h, and then with anti-OSMR beta (R&D Systems, no. AF662, 1:100) antibody (10 µg ml^{-1}) in blocking solution overnight at 4 °C. Sections were washed with PBS and incubated in blocking solution containing anti-goat IgG H&L horseradish peroxidase-conjugated secondary antibody (abcam, no. ab6885, 1:1,000) for 1 h. Finally, sections were stained with diaminobenzidine (DAB, abcam, no. ab64238) and counterstained with haematoxylin (Merck, no. 105174).

Adenovirus production and injection

Adenovirus vectors were generated using the Virapower Adenoviral expression system (Invitrogen). Briefly, open reading frames of genes following a CACC sequence were cloned into a pENTR-D-TOPO plasmid and then recombined into a pAd-CMV-DEST adenoviral plasmid using LR clonase II. PacI (Thermo)-digested adenoviral plasmids were transfected into 293A cells using Lipofectamine 2000 (Invitrogen); 293A cells were cultured in DMEM (Sigma, no. 5796), 10% FBS (Invitrogen) and penicillin-streptomycin (Invitrogen). Adenoviral particles were collected from cell culture supernatant following the manufacturer's instructions. For purification and titration, the Adeno-X Maxi Purification and Adeno-X Rapid Titer kits from Clontech were used. Mice were injected unilaterally with 5×10^8 infectious units of Adeno-EDA-A2 or Adeno-OSM into the TA muscle, with the contralateral muscle receiving the same dose of control Adeno-LacZ. Mice were killed 7 days later.

Site-directed mutagenesis

Mouse NIK coding sequence in the pENTR shuttle plasmid was mutated using Phusion high-fidelity polymerase (NEB) and oligonucleotides designed to carry the desired mutations (indicated by lower case letters): mNIK-T561A, F: 5′-CTACATTCCTGGCgCGGAGACCCACATG-3′, R: 5′-CATGTGGGTCTCCGcGCCAGGAATGTAG-3′; mNIK-K431A-K432A, F: 5′-GCTTCCAGTGTGCTGTCgcAgcGGTACGACTCGAGGTG-3′, R: 5′-CAC CTCGAGTCGTACCgcTgcGACAGCACACTGGAAGC-3′. Mutated coding sequences were recombined into the adenoviral plasmid for adenovirus production as described above.

Myoblast culture

Primary myoblasts were isolated from limb muscles of mice (2–3 days old) as previously described[30]. Myoblasts were cultured in Ham's F-10 nutrient mixture (Invitrogen) with 20% FBS (Invitrogen) supplemented with 2.5 ng ml^{-1} basic fibroblast growth factor (Sigma) and penicillin-streptomycin (Invitrogen). For differentiation, myoblasts were then transferred to DMEM (Sigma, no. 5796) supplemented with

horse serum and penicillin-streptomycin (Invitrogen). Myotube cells were differentiated in 2% horse serum for 48 h for protein isolation or in 5% horse serum for 72 h for gene expression and imaging experiments. Adeno-GFP was added to cells at the start of differentiation for fluorescent myotube imaging, performed using a live-cell imager (Zeiss Axiolab live-cell imager). Cells were treated with other adenoviruses after differentiation for 24–48 h. Human skeletal muscle myoblasts (Lonza) were cultured in DMEM/F12-glutamax (Invitrogen) with 20% FBS (Invitrogen), supplemented with 5 ng ml^{-1} basic fibroblast growth factor (Sigma). Cells were differentiated in DMEM/F12-glutamax with 5% horse serum for 72 h. Human myotubes were treated with either recombinant proteins or adenoviruses for 48 h. The diameters of individual myotubes were measured using Image J software, each being measured at three different sites with values averaged.

Immunofluorescence

Cells were fixed with ice-cold 100% methanol at −20 °C for 10 min, incubated in a blocking solution (3% bovine serum albumin + 0.1% Triton X-100 + 10% horse serum) at room temperature for 1 h and then incubated with MyHC antibody (DSHB, MF20, 1:1000) in the blocking solution for 1 h at room temperature. Cells were washed with PBS and incubated with anti-mouse IgG H&L Alexa Fluor 594 secondary antibody (Abcam, ab150116, 1:2000) and DAPI (Cayman, 14285, 1:3000) in the blocking solution for 1 h and mounted using homemade mounting medium. Cells were visualized using fluorescence microscopy (Zeiss). MyHC signal was normalized to the number of myotube nuclei. Fields with similar density of myotubes were chosen.

Immunoblotting

Cells were homogenized in a cell lysis buffer containing 50 mM Tris (pH 7.4), 150 mM NaCl, 1% Triton X-100, 5 mM EDTA and 1 mM PMSF, supplemented with protease inhibitor tablets (Roche) and phosphatase inhibitors (20 mM NaF, 10 mM β-glycerol phosphate, 10 mM $Na_4P_2O_7$ and 2 mM Na_3VO_4). A similar lysis buffer was used for tissue samples in which 1% NP40 was used as the detergent and 10% glycerol added. Tissues were homogenized using a Kinematica (PT1200E) homogenizer. Homogenates were centrifuged at 13,000 rpm for 10 min and the supernatants used as lysates. Protein concentration was determined by Bio-Rad Protein assay, and 30 μg of protein lysate was used in each SDS–polyacrylamide gel electrophoresis run. For the detection of endogenous NIK protein and its mobility shift, 90 μg of protein lysate was loaded. Nitrocellulose membrane was blotted with the following primary antibodies at 1:1,000 dilution in Tris buffered saline containing 0.05% Tween and 5% bovine serum albumin: Cell Signaling: p65-RelA, (no. 8242), phospho-p65-RelA-Ser536 (no. 3033), p105/p50-NFκB (no.12540), phospho-p105-NFκB-Ser932 (no. 4806), p100/p52-NFκB2 (no. 4882), IκB (no. 4814), phospho-IκB-Ser32 (no. 2859), NIK (no. 4994), JNK (no. 9252), phospho-JNK-Thr183/Tyr185 (no. 4668) and anti-Flag/DYKDDDDK (no. 2368); ECM Bioscience: Atrogin1 (no. AP2041) and MuRF1 (no. MP3401); and DSHB: MyHC antibody (no. MF20). For secondary antibody incubation, Tris buffered saline-T containing 5% milk was used (Cell Signaling: anti-rabbit (no. 7074, 1:2,000) and anti-mouse (no. 7076, 1:2,000)). WesternBright blotting substrates from Advansta were used for visualization of results on a Chemidoc imaging system (Bio-Rad). For blots visualized with a Licor Odyssey CLx imaging system, IRDye 680RD anti-mouse (no. 926-68070, 1:15,000) and IRDye 800CW anti-rabbit (no. 926-32211, 1:15,000) secondary antibodies were used. Uncropped and unprocessed images of all immunoblots are shown in Supplementary Fig. 1.

In vitro phosphatase assay

A cell lysis buffer similar in composition to that described above, but lacking EDTA and phosphatase inhibitors, was used to collect cells. The protein concentration of homogenate supernatants was determined by Bio-Rad Protein assay: 90 μg of lysate was mixed with or without alkaline phosphatase (0.1 U μg^{-1} lysate) and its buffer (Thermo) and incubated at 37 °C for 1 h. Samples were run on SDS–polyacrylamide gel electrophoresis and processed as described above.

RT-qPCR

Total RNA from cultured cells or tissue samples was extracted using Qiazol reagent (Qiagen) and purified with RNA spin columns (Ecotech). Tissues were homogenized using TissueLyzer LT (Qiagen). Complementary DNA synthesis was carried out with a High-Capacity cDNA Reverse Transcription kit (Thermo). The resultant cDNA was analysed by RT-qPCR using a CFX Connect instrument (Bio-Rad). In each reaction, 25 ng of cDNA and 150 nmol of each primer were mixed with iTaq Universal SYBR Green Supermix (Bio-Rad). Relative mRNA levels were calculated by the ΔΔCt method and normalized to cyclophilin mRNA. The following primers were used: *Cyclo* F: 5′-GGAGATGGCACAGGAGGAA-3′, R: 5′-GCCCGTAGTGCTTCAGCTT-3′. *Atrogin1* F: 5′-TCAGAGAGGCAGATTCGCAA-3′, R: 5′-GGGTGACCCCATACTGCTCT-3′. *MuRF1* F: 5′-TCCTGATGGAAACGCTATGGAG-3′, R: 5′-ATTCGCAGCCTGGAAGATGT-3′. *Eda2r* F: 5′-TCCCCTCTACTGGACCTGAA-3′, R: 5′-TGAAAGAGACCTTTCTAGTTCACCT-3′. *Eda2r*-KO F: 5′-CAGGACCAAGAATGCATCCCA-3′, R: 5′-GCTCAACTGGAAGGTACACTGAA-3′. *Eda-a2* F: 5′-TCAAAAATGATCTTTCAGGTGGAG-3′, R: 5′-TGAAGTTGATGTAGTAGACCTG-3′. *Edar* F: 5′-TTGTTGAAGGTCTCAGCCCC-3′, R: 5′-TTTTCACGACCGCCTTCTCA-3′. *Eda-a1* F: 5′-TCTTTCAGGTGGAGTGCTCA-3′, R: 5′-TGAAGTTGATGTAGTAGACTTCTAC-3′. *Nik* F: 5′-CGAGCTACTTCAACGGGGTC-3′, R: 5′-GGCAATGTCTCCCACCTTGA-3′. *Nik*-KO F: 5′-TGTTCTGTGGGAAGTGGGAG-3′, R: 5′-CTCTTGGCTATTCTCACATTCAGC-3′. *Nfkb1* F: 5′-CTGAACAATGCCTTCCGGCT-3′, R: 5′-TGGTACCCCCAGAGACCTCAT-3′. *Nfkb2* F: 5′-CCTTCGTAGTTACAAGCTGGC-3′, R: 5′-GGCACTGTCTTCTTTCACCT-3′. *Nfkbia* F: 5′-TAGCAGTCTTGACGCAGACC-3′, R: 5′-CGTGTGGCCATTGTAGTTGG-3′. *Nfkbib* F: 5′-ACCTCAATAAACCGGAGCCTAC-3′, R: 5′-CACCGGCTTTCAGGAGAAGTT-3′. *Nfkbid* F: 5′-CAGTCATACAAGCCAGGAGAT-3′, R: 5′- TCATATTAACAAAGGCCCGCA-3′. *Nfkbie* F: 5′-GACATTGATGTACAGGAGGGCA-3′, R: 5′-GGTGTGCACCCGTTAAGCAT-3′. *Nfkbiz* F: 5′-CAGTGGAGGCAAAGGATCGTA-3′, R: 5′-GGCAACTCCAAAAAGAGGCG-3′. *Rela* F: 5′-GATCGCCACCGGATTGAAGA-3′, R: 5′-GGGGTTCAGTTGGTCCATTG-3′. *Relb* F: 5′-TTCAAAACGCCACCCTACGA-3′, R: 5′-ACACCGTAGCTGTCATGATCC-3′. *Relc* F: 5′-ATTTATGACAACCGTGCCCCA-3′, R: 5′-CCCTGACACTTCCACAGTTCT-3′. *Ampd3* F: 5′-CTCCTCTCAGCAACAACAGCC-3′, R: 5′-CTCCATGAGCGCTTCCTTTGTG-3′. *Osmr* F: 5′-GGTCCTTCATCCAGCCTTCC-3′, R: 5′-GCTCCTCCAAGACTTCGCTT-3′. *Socs3* F: 5′-TAGACTTCACGGCTGCCAAC-3′, R: 5′-CGGGGAGCTAGTCCCGAA-3′. *Tnf* F: 5′-CCACCACGCTCTTCTGTCTA-3′, R: 5′-CCATTTGGGAACTTCTCATCCC-3′. *Il6* F: 5′-CACTTCACAAGTCGGAGGCT-3′, R: 5′-TGCCATTGCACAACTCTTTTCT-3′. *Ifng* F: 5′-CTTCAGCAACAGCAAGGCG-3′, R: 5′-CTGTGGGTTGTTGACCTCAAACT-3′. *Il1b* F: 5′-AAGGAGAACCAAGCAACGACA-3′, R: 5′-TTGGGATCCACACTCTCCAGC-3′. *Il10* F: 5′-GTAGAAGTGATGCCCCAGGC-3′, R: 5′-GGGGAGAAATCGATGACAGC-3′. *Ccl2* F: 5′-CACTCACCTGCTGCTACTCA-3′, R: 5′-GCTTGGTGACAAAAACTACAGC-3′. *Ccl5* F: 5′-TGCCCACGTCAAGGAGTATT-3′, R: 5′-TTCGAGTGACAAACACGACTG-3′. *F4/80* F: 5′-CTTCTGGGGAGCTTACGATGG-3′, R: 5′-GGCCAAGGCAAGACATACCA-3′. *Cd68* F: 5′-ACTTCGGGCCATGTTTCTCT-3′, R: 5′-GGGGCTGGTAGGTTGATTGT-3′. *Nos2* F: 5′-CAGGAGATGGTCCGCAAGAG-3′, R: 5′-GTCCTGAACGTAGACCTTGGG-3′. *Arg1* F: 5′-CGTAGACCCTGGGGAACACTAT-3′, R: 5′-TCCATCACCTTGCCAATCCC-3′. *Cd163* F: 5′-GTGTTCCGAAGGACAGGTGG-3′, R: 5′-AAGCTGGCCACTTGCTATGC-3′. *Cd19* F: 5′-GAAGCATCCTCGCTTGGGTC-3′, R: 5′-ACTGGGACCGGACTGAATTG-3′. *Cd3e* F: 5′-TGTATCACTCTGGGCTTGCTG-3′, R: 5′-CTCCTTGTTTTGCCCTCTGGG-3′. h*CYCLO* F: 5′-GGAGATGGCACAGGAGGAA-3′, R: 5′-GCCCGTAGTGCTTCAGTTT-3′. h*NIK* F: 5′-GGGACGTCAAAGCTGACAAC-3′, R: 5′-GACACACAGCATGGCCAAAG-3′. h*EDA2R* F: 5′-TGCCTCCTATACTGGAGCTGA-3′, R: 5′-GGGGCCCAAGAGACCTCATTA-3′. h*ATROGIN1* F: 5′-AGG

AAGTACTAAAGAGCGCCA-3′, R: 5′-GCAGGCCGGACCACGTA-3′. h*MURF1* F: 5′-GCCCCATTGCAGAGTGTCTT-3′, R: 5′-ACTGTTCTCCTTG GTCACTCG-3′. h*NFKB2* F: 5′-TCTGCAACTGAAACGCAAGC-3′, R: 5′-CCTC TTCCTTGTCTTCCACCA-3′. h*RELB* F: 5′-CTCGCGACCATGACAGC TAC-3′, R: 5′-GGCTTTTTCTTCCGCCGTTT-3′.

Human gene expression analysis

Patients were enrolled in the ACTICA study, a cross-sectional study aimed at assessing cachexia in patients diagnosed with colorectal or lung cancer. The study was performed at Cliniques Universitaires Saint-Luc, Brussels, Belgium from January 2012 to March 2014. The study protocol was approved by the local ethical committee of Université Catholique de Louvain (protocol code no. 2011/19AVR/157, approved 9 May 2011) and informed written consent was obtained from individuals before entry into the study. The inclusion and exclusion criteria were precisely described previously in the original paper[31]. Cachexia was defined, according to the definition proposed by Fearon et al.[32], as either (1) involuntary weight loss of over 5% over the past 6 months, (2) weight loss of over 2% and body mass index below 20 kg m^{-2} or (3) weight loss of over 2% and low muscularity. Among 152 patients enrolled in the study, skeletal muscle microbiopsy was performed in 35 under general anaesthesia immediately before surgery for cancer and before any other therapeutic intervention. Microbiopsies were taken from the vastus lateralis of the quadriceps with a 14-gauge, true-cut biopsy needle (Bard Magnum Biopsy gun, Bard, Inc.). Muscle samples were cleaned of gross blood contamination and fat or fibrous tissue before being frozen in liquid nitrogen and stored at −80 °C until RNA extraction. Total RNA was extracted from frozen muscle samples using TriPure Isolation Reagent (Roche Diagnostics), as described by the manufacturer. Reverse transcription was performed as described by Gueugneau et al.[33].

Gene expression profiles of rectus abdominis muscle biopsies from patients with cachectic and non-cachectic pancreatic ductal adenocarcinoma and from non-cancer individuals were accessed from the Gene Expression Omnibus (GEO) database with accession no. GSE130563 (ref. 34). Differential gene expression analysis was performed by GEO2R with default settings. One sample from GSE130563 was identified as an outlier (GSM3743567) for EDA2R expression according to Grubbs' test (alpha = 0.0001) and was excluded from the analysis. Gene expression profiles of quadriceps muscle biopsies collected from non-cancer individuals, and from patients with cachectic upper gastrointestinal cancer before and after tumour resection, were accessed from the GEO database (accession no. GSE34111)[35] and analysed by GEO2R using default settings. Gene expression profiles of skeletal muscle samples from both patients with DMD and normal individuals were accessed with accession no. GSE1007 (ref. 36). Samples grouped as DMD and normal were analysed by GEO2R using default settings. RNA sequencing results of muscle biopsy samples from individuals with FSHD were also accessed from the GEO database (accession no. GSE115650)[37]. One-year follow-up gene expression assessment of muscle biopsies from the same patients was also analysed (accession no. GSE140261)[38]. Gene count normalization and fold change calculations were performed using the R package DEseq2 (v.1.34.0).

Statistical analysis

Values are expressed as mean ± s.e.m. Error bars (s.e.m.) shown in all results were derived from biological replicates. Significant differences between two groups were evaluated using a two-tailed *t*-test. Comparisons of more than two groups were performed using either one- or two-way ANOVA and corrected for multiple comparisons using Tukey's post hoc test. Values of $P < 0.05$ were considered statistically significant. Exact *P* values and the type of statistical test used in each experiment can be found in the figure legends.

Reporting summary

Further information on research design is available in the Nature Portfolio Reporting Summary linked to this article.

Data availability

Human gene expression datasets analysed in this study are available in the GEO database: GSE130563 (ref. 34), GSE34111 (ref. 35), GSE1007 (ref. 36), GSE115650 (ref. 37) and GSE140261 (ref. 38). A detailed description of muscle biopsies from patients with cancer used in this study was previously published[31]. Source Data are provided with this paper.

29. Brightbill, H. D. et al. Conditional deletion of NF-kappaB-inducing kinase (NIK) in adult mice disrupts mature B cell survival and activation. *J. Immunol.* **195**, 953–964 (2015).
30. Springer, M. L., Rando, T. A. & Blau, H. M. Gene delivery to muscle. *Curr. Protoc. Hum. Genet.* https://doi.org/10.1002/0471142905.hg1304s31 (2002).
31. Loumaye, A. et al. Role of activin A and myostatin in human cancer cachexia. *J. Clin. Endocrinol. Metab.* **100**, 2030–2038 (2015).
32. Fearon, K. et al. Definition and classification of cancer cachexia: an international consensus. *Lancet Oncol.* **12**, 489–495 (2011).
33. Gueugneau, M. et al. Increased Serpina3n release into circulation during glucocorticoid-mediated muscle atrophy. *J. Cachexia Sarcopenia Muscle* **9**, 929–946 (2018).
34. Judge, S. M. et al. Skeletal muscle fibrosis in pancreatic cancer patients with respect to survival. *JNCI Cancer Spectr.* **2**, pky043 (2018).
35. Gallagher, I. J. et al. Suppression of skeletal muscle turnover in cancer cachexia: evidence from the transcriptome in sequential human muscle biopsies. *Clin. Cancer Res.* **18**, 2817–2827 (2012).
36. Haslett, J. N. et al. Gene expression profiling of Duchenne muscular dystrophy skeletal muscle. *Neurogenetics* **4**, 163–171 (2003).
37. Wang, L. H. et al. MRI-informed muscle biopsies correlate MRI with pathology and DUX4 target gene expression in FSHD. *Hum. Mol. Genet.* **28**, 476–486 (2019).
38. Wong, C. J. et al. Longitudinal measures of RNA expression and disease activity in FSHD muscle biopsies. *Hum. Mol. Genet.* **29**, 1030–1043 (2020).

Acknowledgements We gratefully acknowledge the use of the animal facility infrastructure at Koc University Research Centre for Translational Medicine. We thank M. Kracht (JLU Giessen) for sharing human NIK plasmids and S.-C. Sun (MD Anderson Cancer Center) for sharing NIK-floxed mice. EDA2R-null and NIK-floxed mice were provided by Genentech. We also thank I. Oguz for assistance. D.H.A. was funded by a TUBITAK-BIDEB scholarship. This work was supported by the Scientific and Technological Research Council of Turkey (grant nos. 118Z167, 118Z791, 118C014 and 122Z163) and by EMBO Installation Grant no. 4162 to S.K.

Author contributions S.K. conceived and designed the experiments. S.N.B., A.D. and S.K. performed myotube culture experiments, including RT-qPCR analysis and immunoblotting. S.N.B. and A.D. performed fluorescence microscopy imaging of myotubes and measurement of their diameter. With the assistance of D.H.A., A.D. performed MyHC staining of myotubes and intensity measurements. A.D. conducted immunohistochemistry staining. B.T., S.K., B.Z.C.W. and S.N.B. prepared adenovirus vectors. B.T. and S.K. purified adenoviruses and performed cell culture and mouse experiments involving adenoviruses, including RT-qPCR analysis and immunoblotting. S.N.B. and S.K. performed in vitro phosphatase assays and site-directed mutagenesis studies. S.N.B., A.D. and S.K. conducted tumour inoculation experiments, tissue collection and grip strength measurements. B.Z.C.W. contributed to tissue harvests. S.N.B. and A.D. performed RT-qPCR analysis and immunoblotting of tissue samples. S.N.B. and A.D. conducted tissue histology and S.A. performed quantification of sections. Z.O. performed genotyping of all transgenic mice. J.-P.T. and A.L. supervised and performed muscle biopsy collection from patients with cancer. P.L. performed cDNA library preparation from RNA samples of muscle biopsies. S.N.B. performed qPCR analysis of human cDNA. S.A. conducted all statistical analyses and analysis of gene expression datasets. S.N.B., A.D. and S.K. wrote the manuscript.

Competing interests The authors declare no competing interests.

Additional information

Supplementary information The online version contains supplementary material available at https://doi.org/10.1038/s41586-023-06047-y.

Correspondence and requests for materials should be addressed to Serkan Kir.

Peer review information *Nature* thanks Andreas Bergthaler, Pascal Schneider and the other, anonymous, reviewer(s) for their contribution to the peer review of this work. Peer reviewer reports are available.

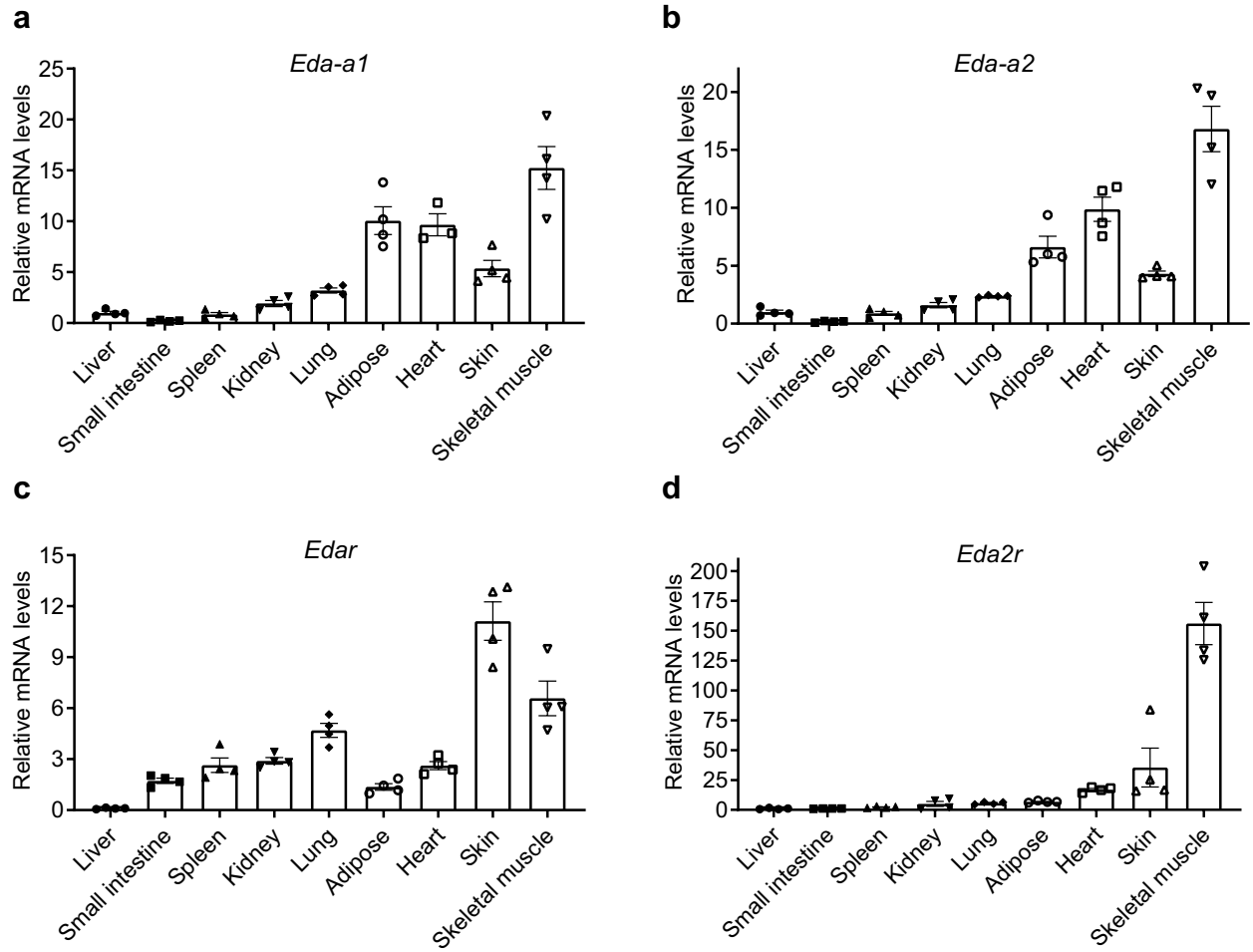

Extended Data Fig. 1 | The expression of *Eda-a2* and *Eda2r* is enriched in skeletal muscle tissue. a-**d**, Various tissue samples were collected from C57BL/6 mice. Relative mRNA levels were determined by RT-qPCR (n = 4 mice). The values are mean ± SEM. Each dot represents a biological replicate. Data are representative of two independent experiments (**a**–**d**).

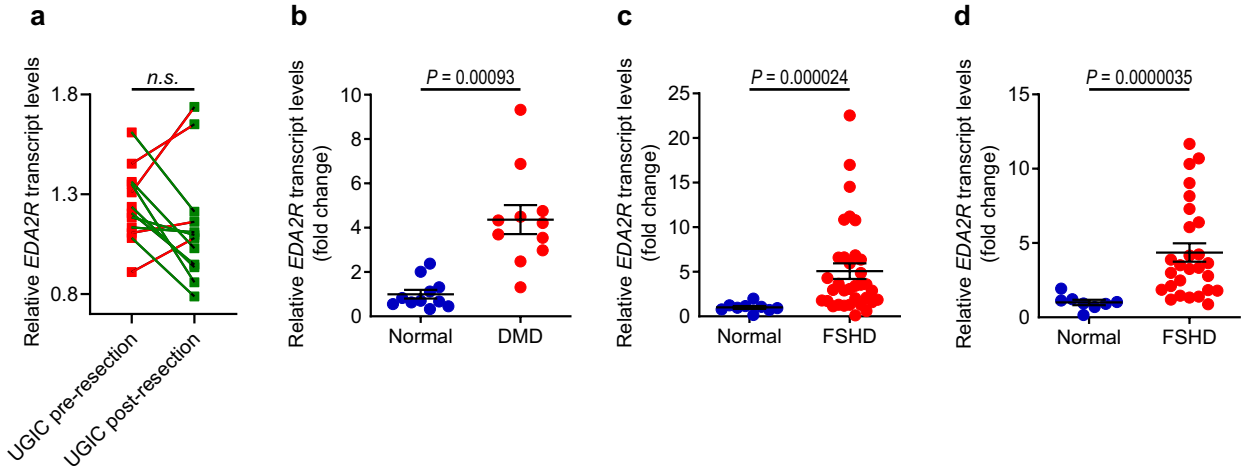

Extended Data Fig. 2 | *EDA2R* expression is induced in DMD and FSHD patients. a, *EDA2R* transcript levels were analyzed in quadriceps muscle biopsies collected from cachectic patients with upper gastrointestinal cancer (n = 12) before and after tumor resection (GSE34111). Upon surgery, EDA2R levels were upregulated in 4 patients (red connecting lines) and downregulated in 8 patients (green connecting lines). n.s. statistically not significant. **b**, GSE1007 dataset was analyzed by GEO2R and *EDA2R* expression values were determined in normal subjects and DMD patients (n = 10). In each group, one individual had 2 technical replicates making the total number of data points 11. **c**, GSE115650 dataset was analyzed by DESeq2 and *EDA2R* expression values were determined in normal subjects (n = 9) and FSHD patients (n = 34). **d**, GSE140261 dataset was analyzed by DESeq2 and *EDA2R* expression values were determined in normal subjects (n = 8) and FSHD patients (n = 27). The values are mean ± SEM. Statistical analysis was conducted using the two-tailed paired *t*-test (**a**). Adjusted *P* values were calculated with Benjamini & Hochberg false discovery rate method by GEO2R (**b**,**c**) and DESeq2 (**d**).

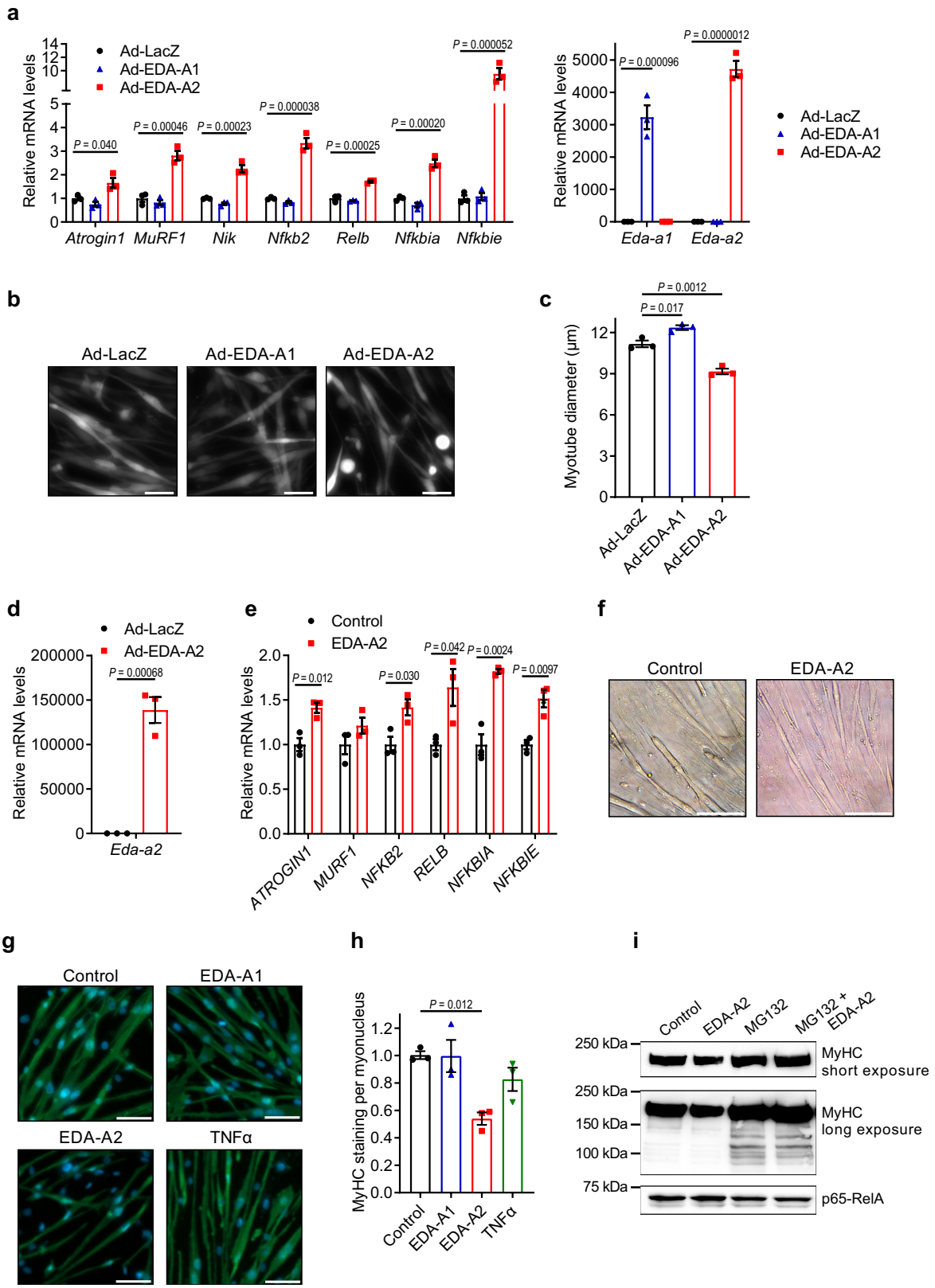

Extended Data Fig. 3 | See next page for caption.

Extended Data Fig. 3 | The overexpression of EDA-A2 or the administration of recombinant EDA-A2 in human and mouse myotubes stimulates cellular atrophy. a–**c**, Mouse primary myotubes were transduced with LacZ, EDA-A1, or EDA-A2 expressing adenoviruses. 24 hr later, gene expression was tested by RT-qPCR (n = 3) (**a**). Myotubes also treated with GFP adenovirus were visualized 48 hr later under the fluorescence microscope. The scale bar is 50 µm (**b**). Average myotube diameter was measured (n = 3) (**c**). **d**–**f**, Human Skeletal Muscle Myoblasts (HSMM) were differentiated into myotubes and treated with an adenovirus expressing EDA-A2 (**d**) or recombinant EDA-A2 protein (250 ng/ml) (**e**,**f**) for 48 hr. Gene expression was determined by RT-qPCR (n = 3) (**d**,**e**). Human myotubes were investigated under the light microscope. The scale bar is 100 µm (**f**). **g**,**h**, Mouse primary myotubes were treated with recombinant EDA-A1, EDA-A2 or TNFα proteins (250 ng/ml each) for 48 hr. MyHC was immunofluorescently labeled while nuclei was counterstained with DAPI. The scale bar is 50 µm (**g**). MyHC signal was normalized to the number of myotube nuclei (n = 3) (**h**). **i**, Mouse primary myotubes treated with recombinant EDA-A2 (250 ng/ml) and proteasome inhibitor MG132 (10 µM) were lysed and protein samples were studied by western blotting. The values are mean ± SEM. Each dot represents a biological replicate. Data are representative of two (**a**–**d**,**f**–**i**) or three (**e**) independent experiments. Statistical analysis was conducted using one-way ANOVA with Tukey's multiple-comparison test (**a**,**c**,**h**) or the two-tailed unpaired *t*-test (**d**,**e**).

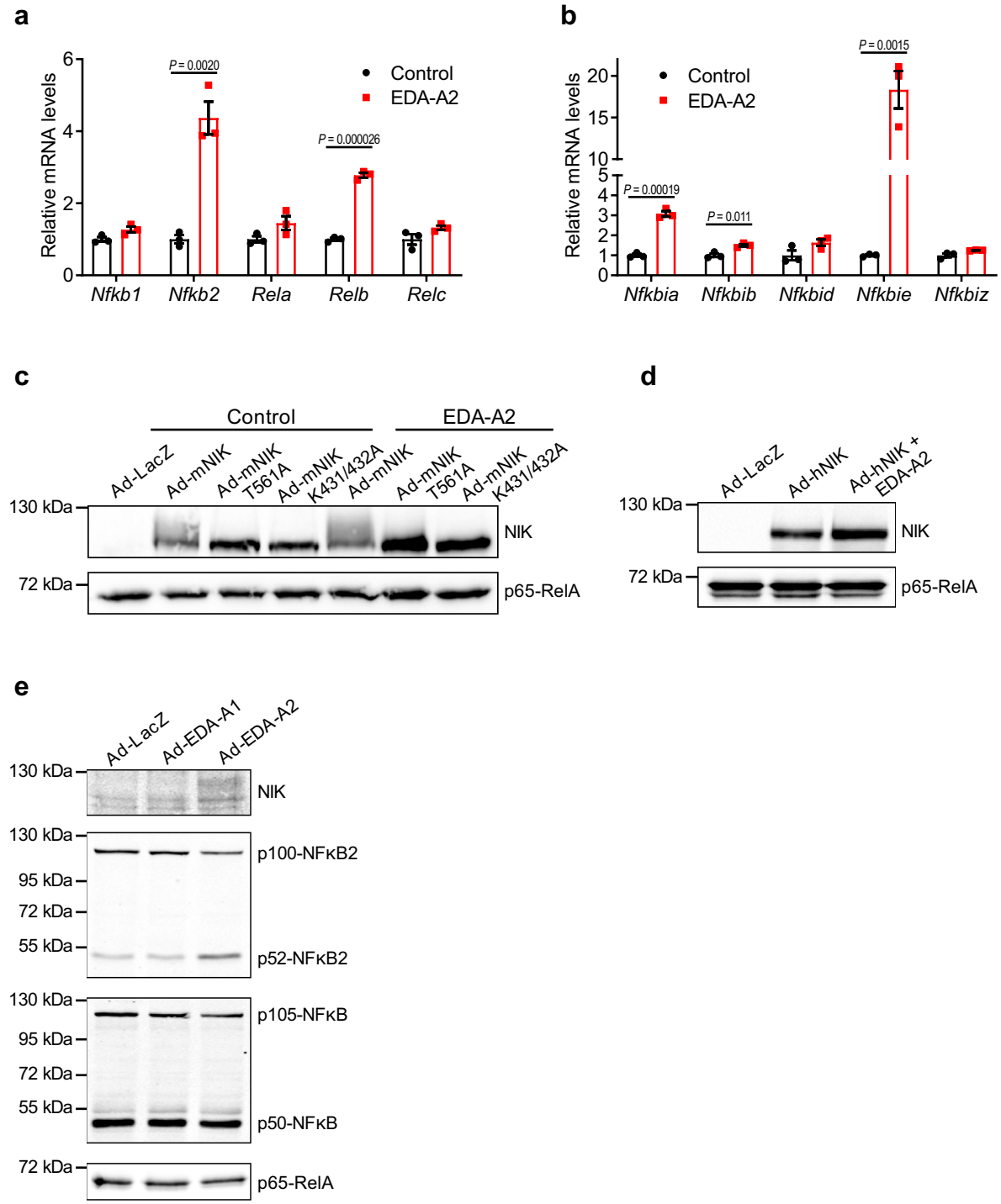

Extended Data Fig. 4 | EDA-A2 stimulates the expression of NFκB signaling components and the alternative NFκB activation in primary myotubes. Electrophoretic mobility shift of mouse NIK protein depends on its autophosphorylation and kinase activity. a,**b**, Mouse primary myotubes were treated with recombinant EDA-A2 (250 ng/ml) for 24 hr and gene expression was determined by RT-qPCR (n = 3). **c**,**d**, Mouse primary myotubes were transduced with adenoviruses expressing LacZ, wild-type mouse NIK (mNIK), autophosphorylation-deficient mNIK-T561A mutant and kinase-dead mNIK-K431/432A mutant or human NIK (hNIK). A day later, recombinant EDA-A2 (250 ng/ml) was also added for another 24 hr. Protein levels were determined by western blotting. **e**, Mouse primary myotubes were transduced with LacZ, EDA-A1, or EDA-A2 expressing adenoviruses. 24 hr later, protein levels were determined by western blotting. The values are mean ± SEM. Each dot represents a biological replicate. Data are representative of two (**b**,**c**,**e**) or three (**a**,**d**) independent experiments. Statistical analysis was conducted using the two-tailed unpaired *t*-test.

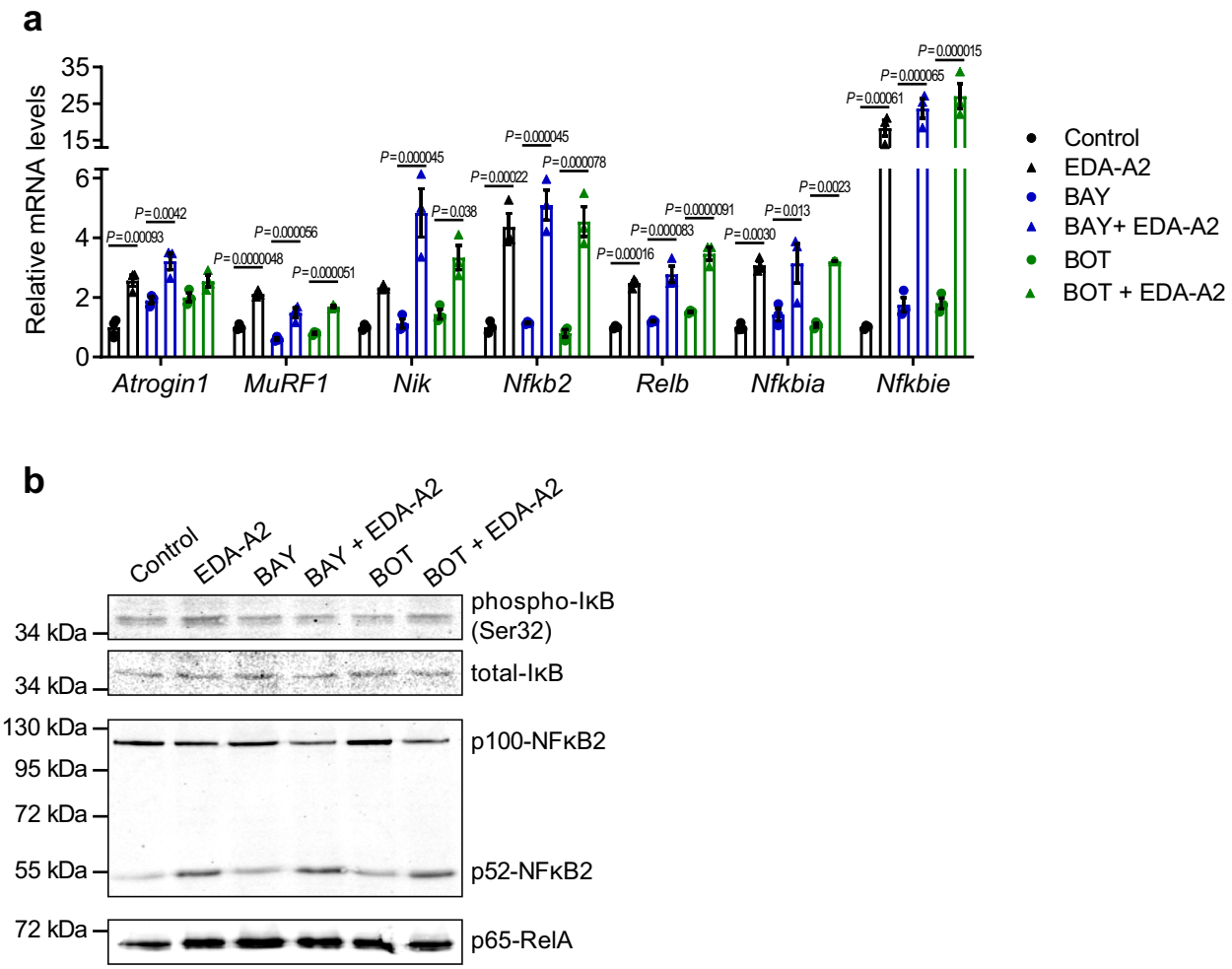

Extended Data Fig. 5 | Activation of the canonical NFκB signaling is dispensable for EDA-A2-induced gene expression in primary myotubes. **a**,**b**, Mouse primary myotubes were treated with IκB phosphorylation inhibitors BAY 11-7082 (10 μM) and BOT-64 (10 μM) in combination with recombinant EDA-A2 (250 ng/ml) for 24 hr. Gene expression was studied by RT-qPCR (n = 3) (**a**) and protein levels were determined by western blotting (**b**). The values are mean ± SEM. Each dot represents a biological replicate. Data are representative of two independent experiments. Statistical analysis was conducted using one-way ANOVA with Tukey's multiple-comparison test.

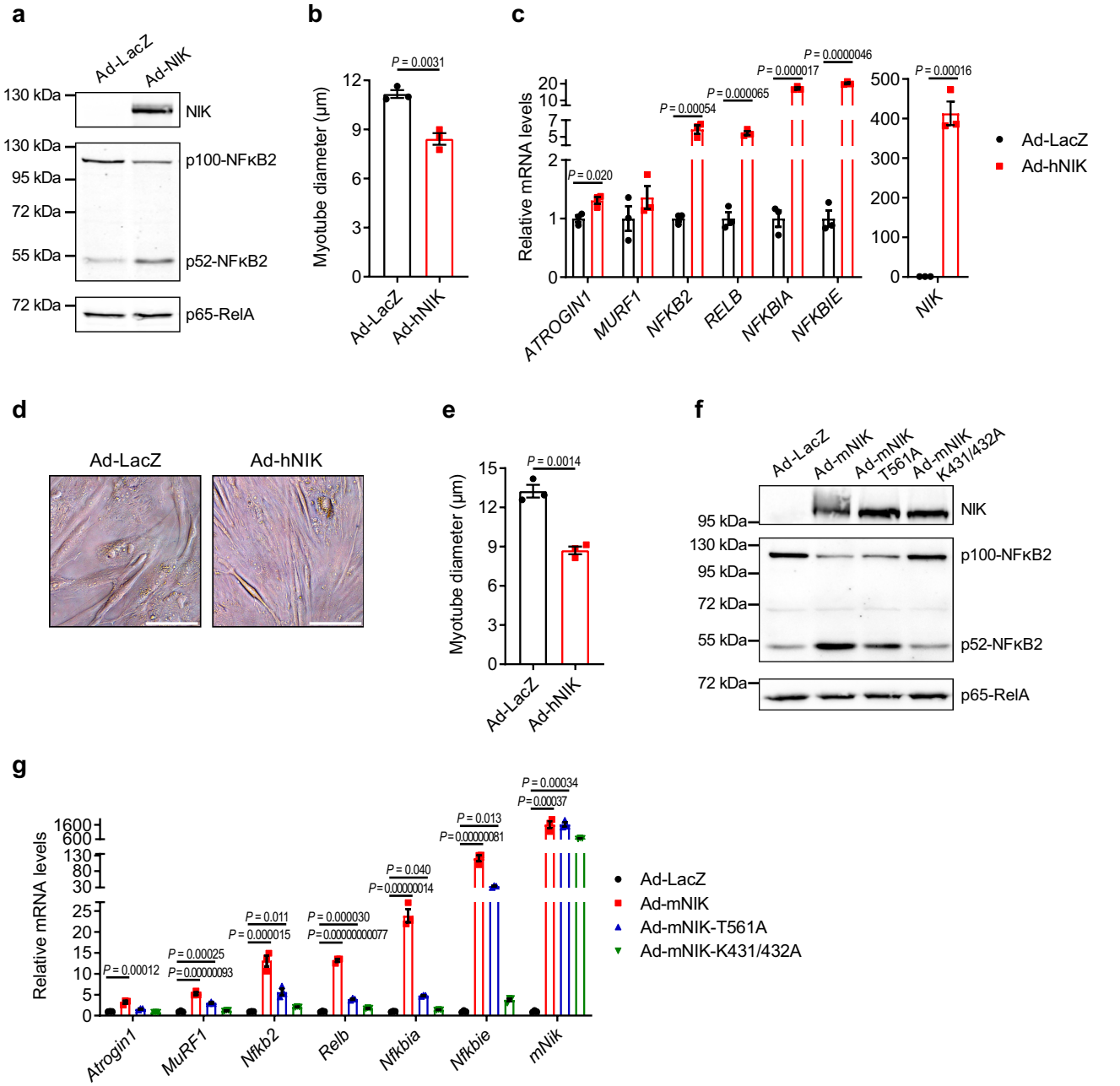

Extended Data Fig. 6 | Overexpression of NIK promotes the alternative NFκB activation and atrophy in primary myotubes. a,**b**, Mouse primary myotubes were transduced with adenoviruses expressing LacZ or human NIK (hNIK). 24 hr later, protein levels were determined by western blotting (**a**). Myotubes also treated with GFP adenovirus were visualized 48 hr later under the fluorescence microscope and average myotube diameter was measured (n = 3) (**b**). **c**–**e**, Human Skeletal Muscle Myoblasts (HSMM) were differentiated into myotubes and treated with adenoviruses expressing LacZ or human hNIK for 48 hr. Gene expression was determined by RT-qPCR (n = 3) (**c**). Human myotubes were investigated under the light microscope. The scale bar is 100 μm (**d**). Myotube diameter was measured (n = 3) (**e**). **f**,**g**, Primary myotubes were transduced with adenoviruses expressing LacZ, mouse NIK (mNIK), autophosphorylation-deficient mNIK-T561A mutant or kinase dead mNIK-K431/432A mutant. Protein levels were determined by western blotting (**f**). This is the same experiment as Extended Data Fig. 4a. NIK and p65-RelA blots were cropped from Extended Data Fig. 4a. mRNA levels were tested by RT-qPCR (n = 3) (**g**). The values are mean ± SEM. Each dot represents a biological replicate. Data are representative of two (**a**,**b**,**d**–**g**) or three (**c**) independent experiments. Statistical analysis was conducted using the two-tailed unpaired *t*-test (**b**,**c**,**e**) and one-way ANOVA with Tukey's multiple-comparison test (**g**).

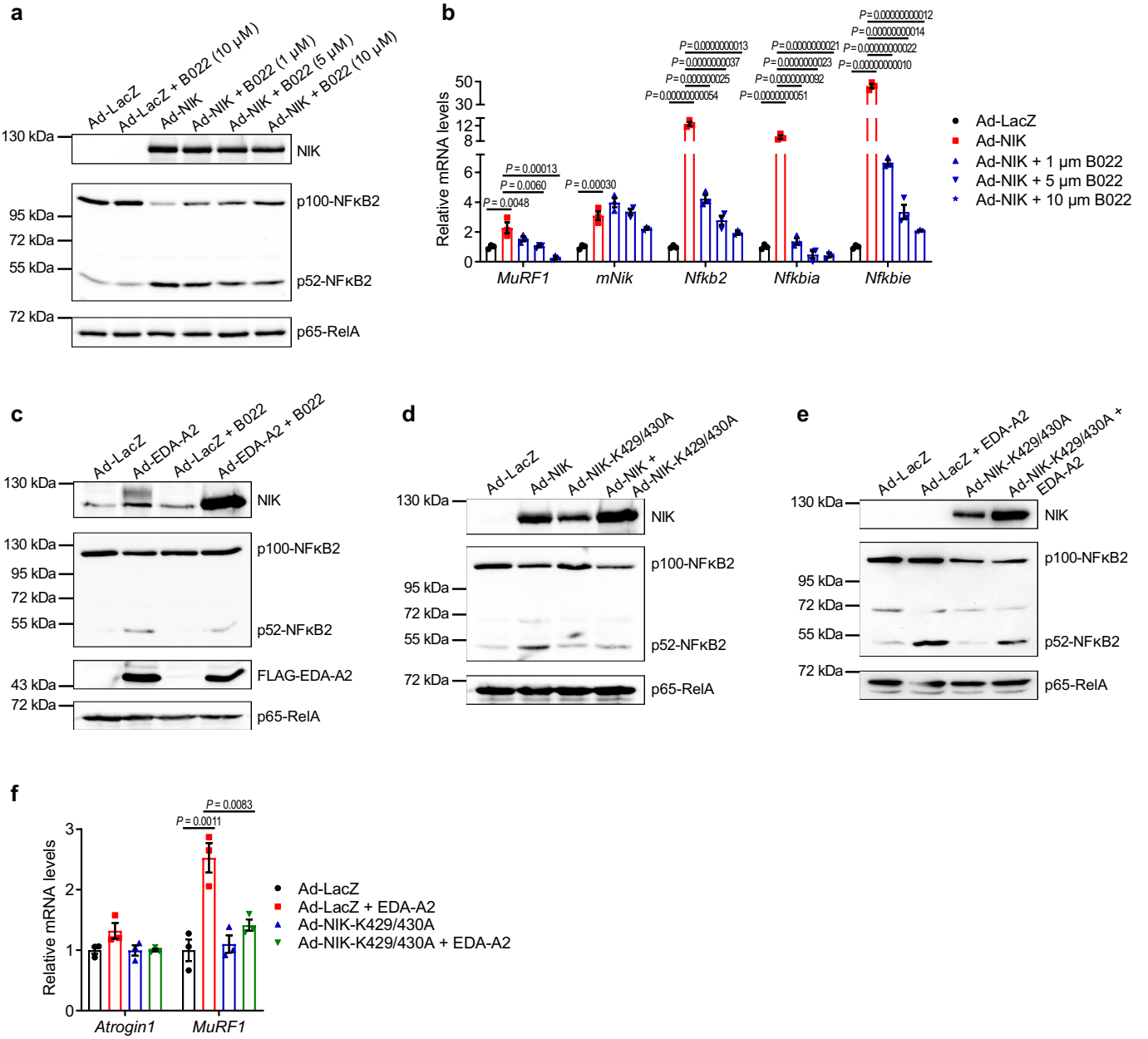

Extended Data Fig. 7 | The inhibition of NIK kinase activity with B022 or a dominant-negative NIK mutant blocks EDA-A2's effects in primary myotubes. a,**b**, Mouse primary myotubes were transduced with adenoviruses expressing LacZ or human NIK and treated with different doses of B022 (1 μM, 5 μM or 10 μM) for 24 hr. Protein levels were determined by western blotting (**a**) and changes in gene expression were tested by RT-qPCR (n = 3) (**b**). **c**, Mouse primary myotubes were transduced with LacZ or EDA-A2 adenoviruses and treated with B022 (5 μM) for 24 hr. Protein levels were determined by western blotting. **d**, Mouse primary myotubes were transduced with adenoviruses expressing wild-type human NIK or the dominant-negative human NIK-K429/430A mutant. Protein levels were determined by western blotting. **e**,**f**, Mouse primary myotubes were transduced with adenoviruses expressing LacZ or the NIK-K429/430A mutant and treated with recombinant EDA-A2 (100 ng/ml) for 24 hr. Protein levels were determined by western blotting (**e**) and changes in gene expression were tested by RT-qPCR (n = 3) (**f**). The values are mean ± SEM. Each dot represents a biological replicate. Data are representative of two (**a**–**d**,**f**) or three (**e**) independent experiments. Statistical analysis was conducted using one-way ANOVA with Tukey's multiple-comparison test.

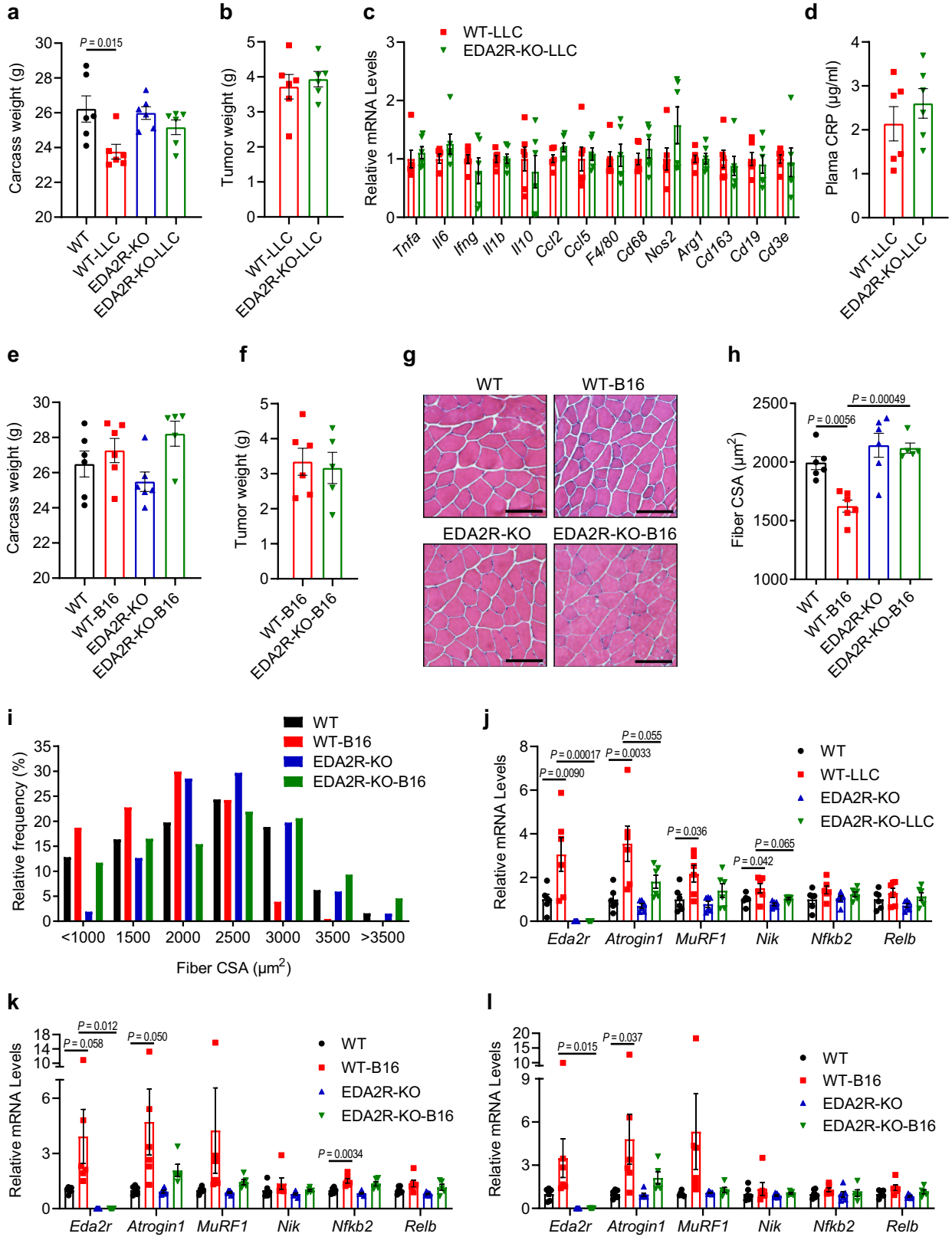

Extended Data Fig. 8 | See next page for caption.

Extended Data Fig. 8 | EDA2R-deficient mice are resistant to tumor-induced muscle wasting. a-**d**,**j**, Mice were inoculated with LLC cells and sacrificed 16 days later (n = 6 mice per group). Carcass weight without the tumor mass (**a**) and tumor weight (**b**) were measured. **c**, Gene expression levels in tumor samples were measured by RT-qPCR (n = 6 mice). **d**, Plasma CRP levels were determined by ELISA (n = 6 mice). **e**–**i**, **k**–**l**, Mice were inoculated with B16 cells and sacrificed 14 days later (EDA2R-KO-B16 n = 5, other groups n = 6 mice). Carcass weight without the tumor mass (**e**) and tumor weight (**f**) were measured. A decrease in carcass weight was induced by LLC tumors. However, tissue wasting was not reflected in the carcass weight when mice received B16 tumors. Because these tumors cause excessive subcutaneous swelling due to inflammation which masks the wasting. **g**–**i**, Gastrocnemius muscle cross-sections were H&E stained (**g**), cross-sectional area (**h**) and the fiber frequency distribution (**i**) were measured. The scale bar is 100 μm. **j**, Quadriceps muscle mRNA levels of the LLC tumor-bearing mice were tested by RT-qPCR (n = 6 mice). **k**,**l**, Gastrocnemius muscle (**k**) and quadriceps muscle (**l**) mRNA levels of the B16 tumor-bearing mice were determined by RT-qPCR (EDA2R-KO-B16 n = 5, other groups n = 6 mice). The values are mean ± SEM. Each dot represents a biological replicate. Data are representative of three independent experiments (**a**–**l**). Statistical analysis was conducted using two-way ANOVA with Tukey's multiple-comparison test (**a**,**h**,**j**,**k**,**l**).

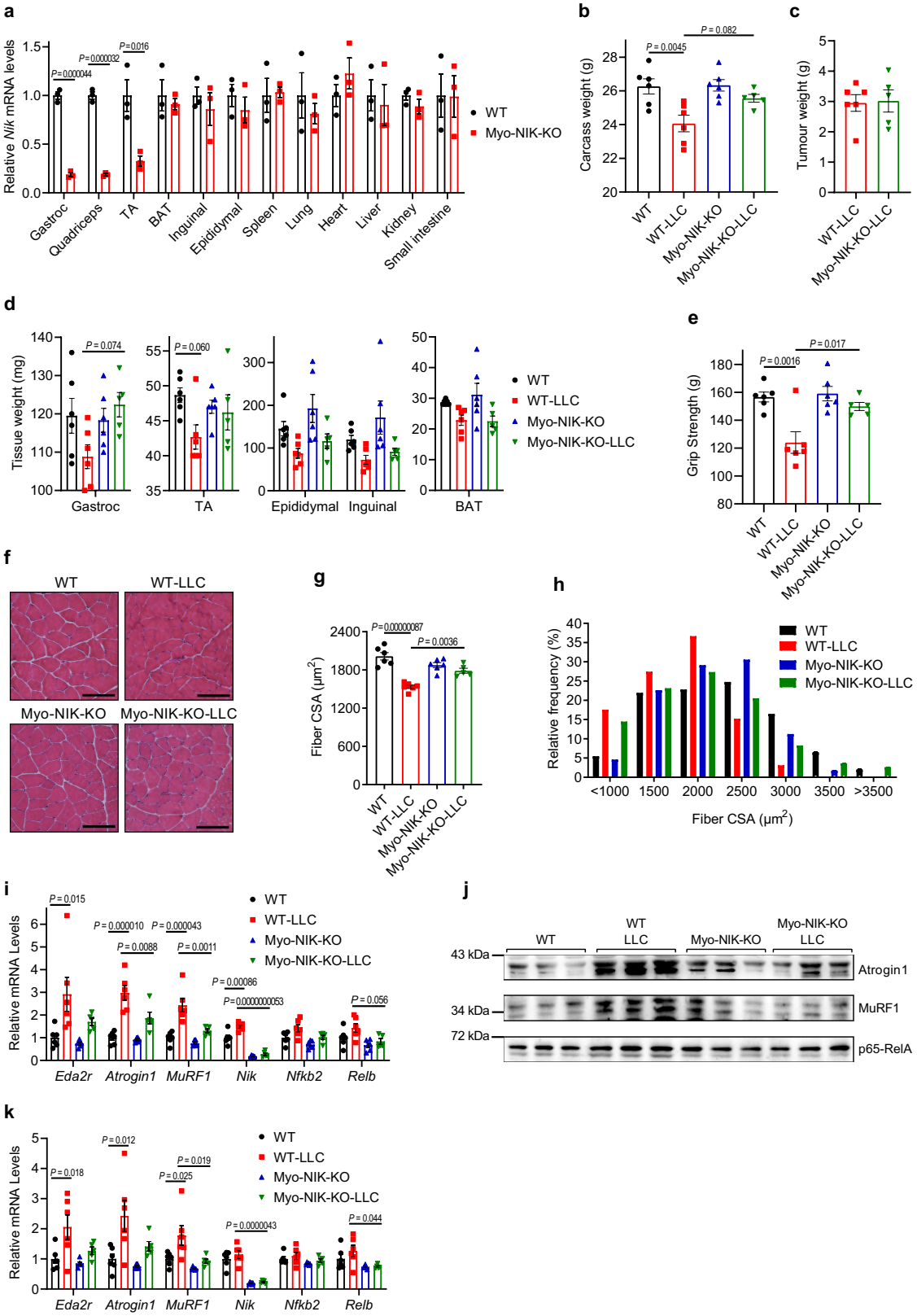

Extended Data Fig. 9 | See next page for caption.

Extended Data Fig. 9 | Muscle-specific depletion of NIK protects from tumor-induced muscle wasting. a. *Nik* mRNA levels were tested by RT-qPCR in various tissues of the Myo-NIK-KO mice (n = 3 mice). **b**–**k**, Mice were inoculated with LLC cells and sacrificed 16 days later (Myo-NIK-KO-LLC n = 5, other groups n = 6 mice). Carcass weight without the tumor mass (**b**) and tumor weight (**c**) were measured. Collected tissues were weighed (**d**). Forelimb grip strength was measured before the sacrifice (**e**). **f**–**h**, Gastrocnemius muscle cross-sections were H&E stained (**f**), cross-sectional area (**g**) and the fiber frequency distribution (**h**) were measured. The scale bar is 100 μm. **i**,**j**, Gastrocnemius muscle mRNA levels were tested by RT-qPCR (Myo-NIK-KO-LLC n = 5, other groups n = 6 mice) (**i**) and their protein levels were determined by western blotting (n = 3 mice) (**j**). Quadriceps muscle mRNA levels were tested by RT-qPCR (Myo-NIK-KO-LLC n = 5, other groups n = 6 mice) (**k**). The values are mean ± SEM. Each dot represents a biological replicate. Data are representative of three independent experiments (**a**–**k**). Statistical analysis was conducted using the two-tailed unpaired *t*-test (**a**) or two-way ANOVA with Tukey's multiple-comparison test (**b**,**d**,**e**,**g**,**i**,**k**).

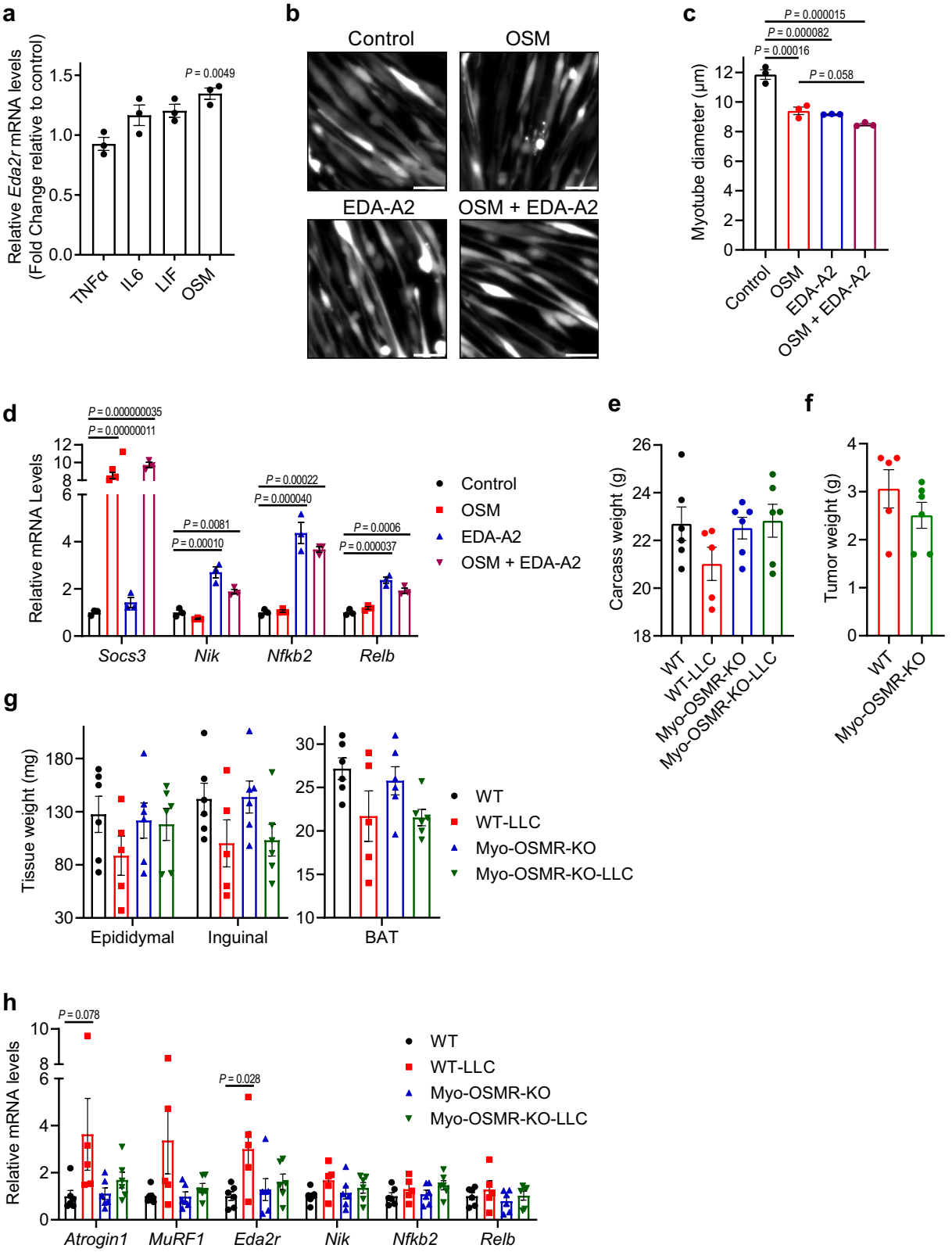

Extended Data Fig. 10 | See next page for caption.

Extended Data Fig. 10 | OSM induces *Eda2r* expression in muscle and the depletion of OSMR protects from muscle wasting. a, Mouse primary myotubes were treated with recombinant TNFα, IL-6, LIF and OSM (250 ng/ml each). mRNA levels were determined by RT-qPCR (n = 3). **b**,**c**, Mouse primary myotubes were treated with recombinant OSM and EDA-A2 (250 ng/ml each) for 48 hr. Myotubes also treated with the GFP adenovirus were visualized under the fluorescence microscope. The scale bar is 50 μm (**b**). Average myotube diameter was measured (n = 3) (**c**). **d**, Mouse primary myotubes were treated with recombinant OSM (250 ng/ml for 48 hr) and EDA-A2 (100 ng/ml for 24 hr). Changes in gene expression were determined by RT-qPCR (n = 3). **e**–**h**, Mice were inoculated with LLC cells and sacrificed 16 days later (WT-LLC n = 5, other groups n = 6 mice). Carcass weight without the tumor mass (**e**) and tumor weight (**f**) were measured. Collected adipose tissues were weighed (**g**). Quadriceps muscle mRNA levels were tested by RT-qPCR (WT-LLC n = 5, other groups n = 6 mice) (**h**). The values are mean ± SEM. Each dot represents a biological replicate. Data are representative of two (**a**–**d**) or three (**e**–**h**) independent experiments. Statistical analysis was conducted using one-way ANOVA with Tukey's multiple-comparison test (**a**,**c**,**d**) and two-way ANOVA with Tukey's multiple-comparison test (**h**).

nature portfolio

Corresponding author(s): SERKAN KIR

Last updated by author(s): Mar 22, 2023

Reporting Summary

Nature Portfolio wishes to improve the reproducibility of the work that we publish. This form provides structure for consistency and transparency in reporting. For further information on Nature Portfolio policies, see our Editorial Policies and the Editorial Policy Checklist.

Statistics

For all statistical analyses, confirm that the following items are present in the figure legend, table legend, main text, or Methods section.

n/a	Confirmed
☐	☒ The exact sample size (*n*) for each experimental group/condition, given as a discrete number and unit of measurement
☐	☒ A statement on whether measurements were taken from distinct samples or whether the same sample was measured repeatedly
☐	☒ The statistical test(s) used AND whether they are one- or two-sided *Only common tests should be described solely by name; describe more complex techniques in the Methods section.*
☒	☐ A description of all covariates tested
☐	☒ A description of any assumptions or corrections, such as tests of normality and adjustment for multiple comparisons
☐	☒ A full description of the statistical parameters including central tendency (e.g. means) or other basic estimates (e.g. regression coefficient) AND variation (e.g. standard deviation) or associated estimates of uncertainty (e.g. confidence intervals)
☐	☒ For null hypothesis testing, the test statistic (e.g. *F*, *t*, *r*) with confidence intervals, effect sizes, degrees of freedom and *P* value noted *Give P values as exact values whenever suitable.*
☒	☐ For Bayesian analysis, information on the choice of priors and Markov chain Monte Carlo settings
☒	☐ For hierarchical and complex designs, identification of the appropriate level for tests and full reporting of outcomes
☒	☐ Estimates of effect sizes (e.g. Cohen's *d*, Pearson's *r*), indicating how they were calculated

Our web collection on statistics for biologists contains articles on many of the points above.

Software and code

Policy information about availability of computer code

Data collection	Image J software (v1.53k) was used to measure myotube diameters and muscle fiber cross-sectional area.
Data analysis	Gene expression datasets were accessed from the Gene Expression Omnibus database. Microarray datasets were analyzed using GEO2R tool of the database using default settings. For RNA sequencing datasets, gene counts normalization and fold change calculations were performed using the DEseq2 (v1.34.0) R package. Statistical analysis was conducted using Jamovi 2.3.18.

For manuscripts utilizing custom algorithms or software that are central to the research but not yet described in published literature, software must be made available to editors and reviewers. We strongly encourage code deposition in a community repository (e.g. GitHub). See the Nature Portfolio guidelines for submitting code & software for further information.

Data

Policy information about availability of data

All manuscripts must include a data availability statement. This statement should provide the following information, where applicable:

- Accession codes, unique identifiers, or web links for publicly available datasets
- A description of any restrictions on data availability
- For clinical datasets or third party data, please ensure that the statement adheres to our policy

Human gene expression datasets analyzed in this study are available in the GEO database; GSE130563 (REF34), GSE34111 (REF35), GSE1007 (REF36), GSE115650 (REF37), GSE140261 (REF38). A detailed description of the cancer patient muscle biopsies used in this study was previously published (REF31).

Field-specific reporting

Please select the one below that is the best fit for your research. If you are not sure, read the appropriate sections before making your selection.

☒ Life sciences ☐ Behavioural & social sciences ☐ Ecological, evolutionary & environmental sciences

For a reference copy of the document with all sections, see nature.com/documents/nr-reporting-summary-flat.pdf

Life sciences study design

All studies must disclose on these points even when the disclosure is negative.

Sample size	For every experiment, sample size was determined empirically (preliminary experiments were performed) to ensure that desired statistical power can be achieved. To determine sample size in mouse experiments, power calculations were done according to methods outlined in Guidelines for the Care and Use of Animals in Neuroscience and Behavioral Research (National Academies Press, 2003). Sample size in mouse experiments was chosen to be at least 4 to ensure that adequate statistical power will be achieved.
Data exclusions	In tumor inoculation experiments, mice were excluded if tumor did not grow and tumor size was less than 1 gram. Mice were excluded from grip strength measurements if they refused to pull the bar attached to the instrument.
Replication	Each experiment was repeated 2 or 3 times. The exact number of independent experiments was stated in the figure legends. All data points presented in this study represent biological replicates.
Randomization	Mice were divided into treatment groups randomly while satisfying the criteria that average body weight in each group is about the same.
Blinding	The investigators were blinded to group allocation during data collection. Group allocation information was not available during data collection and was revealed during data analysis.

Reporting for specific materials, systems and methods

We require information from authors about some types of materials, experimental systems and methods used in many studies. Here, indicate whether each material, system or method listed is relevant to your study. If you are not sure if a list item applies to your research, read the appropriate section before selecting a response.

Materials & experimental systems

n/a	Involved in the study
☐	☒ Antibodies
☐	☒ Eukaryotic cell lines
☒	☐ Palaeontology and archaeology
☐	☒ Animals and other organisms
☐	☒ Human research participants
☒	☐ Clinical data
☒	☐ Dual use research of concern

Methods

n/a	Involved in the study
☒	☐ ChIP-seq
☒	☐ Flow cytometry
☒	☐ MRI-based neuroimaging

Antibodies

Antibodies used	The following antibodies were used in western blotting: p65-RelA (Cell Signaling, #8242), phospho-p65-RelA-Ser536 (Cell signaling, #3033), p105/p50-NFκB (Cell Signaling, #12540), phospho-p105-NFκB-Ser932 (Cell Signaling, #4806), p100/p52-NFκB2 (Cell Signaling, #4882), IκB (Cell Signaling, #4814), phospho-IκB-Ser32 (Cell Signaling, #2859), NIK (Cell Signaling, #4994), JNK (Cell Signaling, #9252), phospho-JNK- Thr183/Tyr185 (Cell Signaling, #4668), anti-Flag/DYKDDDDK (Cell Signaling, #2368), Atrogin1 (ECM Bioscience, #AP2041), MuRF1 (ECM Bioscience, #MP3401), MyHC antibody (DSHB, #MF20), IRDye 680RD anti-mouse (Li-cor Biosciences, #926-68070), IRDye 800CW anti-rabbit (Li-cor Biosciences, #926-32211), anti-rabbit IgG, HRP-linked Antibody (Cell Signaling, #7074), Anti-mouse IgG, HRP-linked Antibody (Cell Signaling, #7076) The following antibodies were used in IF: MyHC antibody (DSHB, MF20), anti-mouse IgG H&L Alexa Fluor 594 (Abcam, ab150116) The following antibodies were used for IHC: OSMR beta (R&D Systems, AF662), donkey anti-goat IgG H&L HRP (Abcam, ab6885)
Validation	All of the primary antibodies used are commercially available and validated by the manufacturer. p65-RelA (Cell Signaling, #8242) https://www.cellsignal.com/products/primary-antibodies/nf-kb-p65-d14e12-xp-rabbit-mab/8242 phospho-p65-RelA-Ser536 (Cell signaling, #3033) https://www.cellsignal.com/products/primary-antibodies/phospho-nf-kb-p65-ser536-93h1-rabbit-mab/3033 p105/p50-NFκB (Cell Signaling, #12540)

https://www.cellsignal.com/products/primary-antibodies/nf-kb1-p105-p50-d7h5m-rabbit-mab/12540

phospho-p105-NFκB-Ser932 (Cell Signaling, #4806)
https://www.cellsignal.com/products/primary-antibodies/phospho-nf-kb-p105-ser932-18e6-rabbit-mab/4806

p100/p52-NFκB2 (Cell Signaling, #4882)
https://www.cellsignal.com/products/primary-antibodies/nf-kb2-p100-p52-antibody/4882

IκB (Cell Signaling, #4814)
https://www.cellsignal.com/products/primary-antibodies/ikba-l35a5-mouse-mab-amino-terminal-antigen/4814

phospho-IκB-Ser32 (Cell Signaling, #2859)
https://www.cellsignal.com/products/primary-antibodies/phospho-ikba-ser32-14d4-rabbit-mab/2859

NIK (Cell Signaling, #4994)
https://www.cellsignal.com/products/primary-antibodies/nik-antibody/4994

JNK (Cell Signaling, #9252)
https://www.cellsignal.com/products/primary-antibodies/sapk-jnk-antibody/9252

phospho-JNK- Thr183/Tyr185 (Cell Signaling, #4668)
https://www.cellsignal.com/products/primary-antibodies/phospho-sapk-jnk-thr183-tyr185-81e11-rabbit-mab/4668

anti-Flag/DYKDDDDK (Cell Signaling, #2368)
https://www.cellsignal.com/products/primary-antibodies/dykddddk-tag-antibody-binds-to-same-epitope-as-sigma-s-anti-flag-m2-antibody/2368

Atrogin1 (ECM Bioscience, AP2041)
https://ecmbio.com/products/ap2041

MuRF1 (ECM Bioscience, MP3401)
https://ecmbio.com/products/mp3401

MyHC antibody (DSHB, #MF20)
https://dshb.biology.uiowa.edu/MF-20

OSMR beta (R&D Systems, AF662)
https://www.rndsystems.com/products/mouse-osmrbeta-antibody_af662

Eukaryotic cell lines

Policy information about cell lines

Cell line source(s)	Mouse primary myoblasts were home-made. LLC, B16-F10 and 293A cells were originally acquired from ATCC. HSMM cells were acquired from Lonza.
Authentication	Cell lines were acquired from ATCC and Lonza and they were not authenticated.
Mycoplasma contamination	Cell lines were tested for mycoplasma. Cells that were myocoplasma positive were treated with Mycozap plus PR until the test result returned to negative.
Commonly misidentified lines (See ICLAC register)	No commonly misidentified lines were used.

Animals and other organisms

Policy information about studies involving animals; ARRIVE guidelines recommended for reporting animal research

Laboratory animals	Mice were housed at 22°C and 50% humidity with a 12 hour light/dark cycle (7am-7pm) and given ad libitum access to a standard rodent chow diet and water. 8-12-week-old male mice were used in all animal experiments. EDA2R-KO and NIK-floxed mice were generated by Genentech (REF8, REF29). Myo-NIK-KO mice were generated by crossing NIK-floxed and ACTA1-Cre mice (Jackson strain #006149). OSMR-floxed mice (strain #011081) were purchased from Jackson laboratory. Myo-OSMR-KO mice were generated by crossing OSMR-floxed and ACTA1-Cre mice (Jackson strain #006149). All mice were maintained on a pure C57BL/6 background.
Wild animals	No wild animals were used in this study.
Field-collected samples	No field collected samples were used in this study.
Ethics oversight	All animal protocols were approved by the Institutional Animal Care and Use Committee of Koc University.

Note that full information on the approval of the study protocol must also be provided in the manuscript.

Human research participants

Policy information about studies involving human research participants

Population characteristics	Patients were enrolled in the ACTICA study, a cross-sectional study aimed at assessing cachexia in patients diagnosed with colorectal or lung cancer. The study information was previously described in the original paper (REF31).
Recruitment	Written consent was given prior to entry into the study. The inclusion and exclusion criteria have been precisely described previously in the original paper (REF31).
Ethics oversight	The study was performed at the Cliniques Universitaires Saint-Luc, Brussels, Belgium from January 2012 to March 2014. The study protocol was approved by the local ethical committee of the Université Catholique de Louvain (protocole code: 2011/19AVR/157, approved on the 9 May 2011).

Note that full information on the approval of the study protocol must also be provided in the manuscript.